ALEPH 95-03
PHYSIC 95-03
D.Rousseau, A.Sadouki and M.Talby
11 January 1995

Measurement of $|V_{cb}|$ and $\overline{B^0} \to D^{*+} l^- \overline{\nu_l}$ branching fraction

D.Rousseau, A.Sadouki and M.Talby

Centre de Physique des Particules de Marseille

Abstract

In a data sample of 1,5 million hadronic Z^0 decays collected with the ALEPH detector in 1991, 1992 and 1993, a total of 170 exclusive semileptonic decays $\overline{B^0} \to D^{*+} l^- \overline{\nu_l}$ have been reconstructed. The D^{*+} meson is reconstructed using the decay channel $D^{*+} \to D^0 \pi^+$, and the D^0 is reconstructed using the two decay modes : $D^0 \to K^- \pi^+$ and $D^0 \to K^- \pi^+ \pi^- \pi^+$. From the differential rate $d\Gamma(\overline{B^0} \to D^{*+} l^- \overline{\nu_l})/dq^2$ of the B meson selected sample, the matrix element $|V_{cb}|$ and the branching fraction $Br(\overline{B^0} \to D^{*+} l^- \overline{\nu_l})$ are measured to be :

$$\eta_A \hat{\xi}(1)|V_{cb}| = 0.0316 \pm 0.0037(stat.) \pm 0.0033(syst.)$$

$$Br(\overline{B^0} \to D^{*+} l^- \overline{\nu_l}) = 6.09 \pm 0.56(stat.) \pm 0.95(syst.)\%$$

1 Introduction

The determination of the CKM matrix elements is one of the experimental inputs to the standard model of electroweak interactions. Our present knowledge of these matrix elements comes from the experimental study of different decay processes. The magnitude of $|V_{cb}|$ can be determined either from inclusive semileptonic B decays or from exclusive channels such as $\overline{B^0} \to D^{*+} l^- \overline{\nu_l}$. Although statistically not limited the inclusive method suffers from theoretical uncertainties such as b quark mass and the quark model used to represent the inclusive semileptonic decays. The exclusive decay $\overline{B^0} \to D^{*+} l^- \overline{\nu_l}$ has much less theoretical limitations. In the framework of the heavy quark effective theory (HQET) [1], this decay mode can be expressed, in the leading order, in terms of only one form factor, the Isgur-Wise function. Although HQET cannot predict the shape of this function, for decays close to zero recoil (decays of maximum q^2)[1], it is absolutely normalized up to corrections of order $1/m_b^2$ [2]. This normalization provides a reliable determination of $|V_{cb}|$ which is, compared to the inclusive method, almost free from theoretical uncertainties. Hence with more data, exclusive semileptonic decays should provide the most accurate measurement of $|V_{cb}|$.

The strategy, commonly used [3], to extract $|V_{cb}|$ from the decay $\overline{B^0} \to D^{*+} l^- \overline{\nu_l}$, is to fit its measured differential decay rate $d\Gamma(\overline{B^0} \to D^{*+} l^- \overline{\nu_l})/dq^2$ and to extrapolate it up to point of maximum q^2. The first measurements of $|V_{cb}|$ with this method were performed by ARGUS and CLEO experiments [4, 5]. At LEP the same method can also be used to measure $|V_{cb}|$ from the differential rate of the decay $\overline{B^0} \to D^{*+} l^- \overline{\nu_l}$. ALEPH has presented this measurement at the Glasgow conference [6]. Although the collected number of B mesons per experiment at LEP is small compared to CLEO experiment [2], its reconstruction is much easier, thanks to the high boost at Z^0 resonance, and hence the reconstruction efficiency is better. In this note we report on a measurement of the differential and the total branching fraction of the decay $\overline{B^0} \to D^{*+} l^- \overline{\nu_l}$ where the D^{*+} meson is reconstructed using the channel $D^{*+} \to D^0 \pi^+$, and the D^0 is reconstructed in the two decay modes : $D^0 \to K^- \pi^+$ and $D^0 \to K^- \pi^+ \pi^- \pi^+$. $|V_{cb}|$ is extracted from a fit to the measured differential decay rate $d\Gamma(\overline{B^0} \to D^{*+} l^- \overline{\nu_l})/dq^2$.

This note is organized as follows. In section 2 we describe the $\overline{B^0} \to D^{*+} l^- \overline{\nu_l}$ selection from hadronic Z^0 decays and reconstruction efficiency. In section 3 the reconstruction of q^2 is presented. In section 4, the background sources are reviewed and the rejection of the physics background component is discribed in detail. The fitting procedure to extract $|V_{cb}|$ from the differential decay rate $d\Gamma(\overline{B^0} \to D^{*+} l^- \overline{\nu_l})/dq^2$ and the branching fraction $Br(\overline{B^0} \to D^{*+} l^- \overline{\nu_l})$

[1] The q^2 is the mass squared of the virtual W, *i.e.* for the decay $\overline{B^0} \to D^{*+} l^- \overline{\nu_l}$, the mass squared of the (l, ν) pair.

[2] For the $|V_{cb}|$ measurement CLEO has used 1,5 million $B\overline{B}$ while in this note we use about 300,000 $b\overline{b}$ events.

is described in section 5 and the results presented. The systematic errors are presented in section 6 and a conclusion in section 7.

2 $\overline{B^0} \rightarrow D^{*+} l^- \overline{\nu_l}$ selection and reconstruction efficiency

The data sample used in this analysis is based on 1,5 million hadronic class 16 events from 1991, 1992 and 1993 (PERF and MAYB) data, with all Heavy Flavour Group selections and VDET fully operational.

2.1 Event selection

Exclusive semileptonic decays $\overline{B^0} \rightarrow D^{*+} l^- \overline{\nu_l}$ are selected in hadronic events where a lepton is associated with a D^{*+} in the same hemisphere. The lepton is identified with the following cuts :

for electrons :

- good charged track[3]
- $P_l > 3$ GeV/c
- $|D0_l| < 0.5$ cm
- $-1.8 < R_2 < 3.0$, $-2.1 < R_3 < 3.0$
- $(\mathrm{dE/dx})_e < -2.5$ and $N_{wires} > 50$ when the dE/dx measurements are available
- Pair conversion rejection (PAIRFD)

and for muons :

- good charged track
- $P_l > 3$ GeV/c
- $|D0_l| < 0.5$ cm
- QMUIDO flag IDF > 12

The D^{*+} is reconstructed using the channel $D^{*+} \rightarrow D^0 \pi^+$, and the D^0 is reconstructed in the two decay modes : $D^0 \rightarrow K^- \pi^+$ and $D^0 \rightarrow K^- \pi^+ \pi^- \pi^+$.

The D^0 selection cuts are :

[3]We use the following definition of a good charged track : $|cos\theta| < 0.95$, $|D0| < 2$ cm , $|Z0| < 10$ cm and at least 4 TPC hits.

- kaon and pions are required to be good charged tracks
- When available the dE/dx measurements are required to be for a kaon candidate consistent within 2 sigma with that expected for kaons and for pion candidates to be consistent within 3 sigma with that expected for pions.
- For $D^0 \rightarrow K^-\pi^+\pi^-\pi^+$ channel, the momentum of the kaon is required to be greater than 2 GeV/c .
- The D^0 vertex fit is required to have Prob(χ^2) > 1%. To insure good vertex reconstruction, the two or two out of the four D^0 tracks are required to have one or more VDET hits in $r\phi$ and z coordinates.

To form a D^{*+}, the D^0 candidate is paired with a soft pion from the same hemisphere, having the right charge and a momentum less than 4.3 GeV/c . Further the mass difference $M_{D^0\pi^+} - M_{D^0}$ is required to be within 2.1 MeV/c^2 of the $D^{*+} - D^0$ mass difference.

Reconstructed D^{*+} candidates are combined with an identified lepton from the same hemisphere and the $D^{*+}l^-$ system is then required to satisfy the following criteria :

- $\theta_{D^{*+}l^-} < 45°$
- $M_{D^{*+}l^-} < 5.3$ GeV/c^2
- D^0l^- vertex fit with Prob(χ^2) > 1%. As for the D^0, to insure good vertex reconstruction the lepton is required to have one or more VDET hits in $r\phi$ and z coordinates.
- the distance of the D^0l^- vertex from the interaction point projected onto the D^0l^- direction is required to be greater than 1 mm. This cut is necessary to ensure a good q^2 reconstruction and an efficient physics background rejection, as described later.
- the distance between the D^0 vertex and the D^0l^- vertex projected onto the D^0 direction is required to be greater than -1 mm.

In what follows, the set of cuts described above will be called basic cuts.

Figure 1 shows the invariant mass distributions of the $D^0 \rightarrow K^-\pi^+$ and the $D^0 \rightarrow K^-\pi^+\pi^-\pi^+$ candidates measured at the D^0 vertex, after the basic cuts. A fit to the two mass distributions with a Gaussian representing the D^0 signal and a second order polynomial for background, yields a D^0 mass and width, consistent with expectations from Monte Carlo simulation. Table 1 summarizes the number of $D^{*+}l^-$ candidates and the number of accidental combinations (called in what follows, see section 4, fake D^0 accidentals) within 2.5 sigma of the D^0 mass, and the D^0 mass and width as obtained from the fit of the two mass distributions.

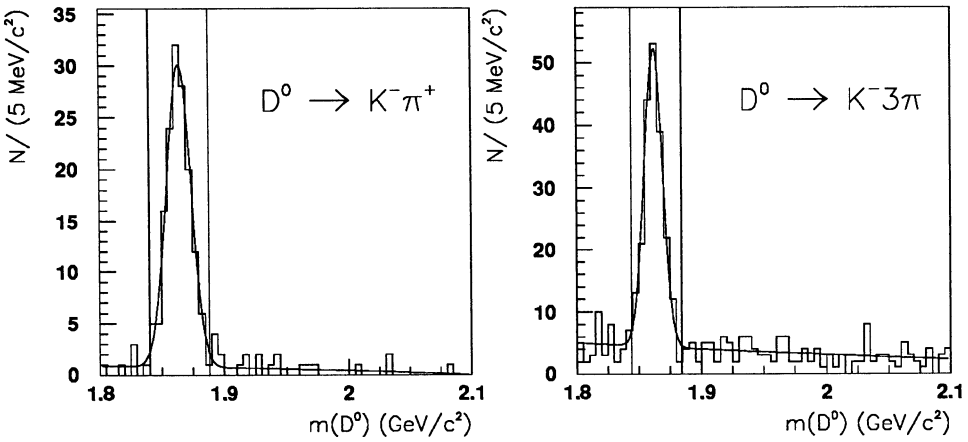

Figure 1: Invariant mass distributions of $D^0 \to K^-\pi^+$ candidates and $D^0 \to K^-\pi^+\pi^-\pi^+$ candidates for $D^{*+}l^-$ events after basic cuts.

Decay process	$N_{D^{*+}l^-}$	fake D^0 accid.	M_{D^0}(MeV/c^2)	$\sigma_{M_{D^0}}$(MeV/c^2)
$D^0 \to K^-\pi^+\pi^-\pi^+$	206.0 ± 14.4	34.7 ± 6.9	1862.0 ± 0.7	7.3 ± 0.6
$D^0 \to K^-\pi^+$	145.0 ± 12.0	6.9 ± 3.1	1864.3 ± 0.9	9.7 ± 0.8
total	351.0 ± 18.7	41.6 ± 7.6	-	-

Table 1: The number of $D^{*+}l^-$ events within 2.5 $\sigma_{M_{D^0}}$ (fake D^0 accidentals included), fake D^0 accidentals and the reconstructed D^0 mass and width after basic cuts.

2.2 Reconstruction efficiency

The reconstruction efficiency is estimated from Monte Carlo generated events processed throught the ALEPH detector and fully reconstructed. The B^0 lifetime τ_{B^0} and the fragmentation function parameter ϵ_b in the Monte Carlo are different from the experimental values [4]. To take into account these differences, Monte Carlo events are weighted so that the simulated B lifetime and B momentum distribution agree with experimental values.

Differences in efficiency between data and Monte Carlo for the two D^0 decay channels used in this analysis, have been investigated for cuts such as the dE/dx cut, the D^0 and $D^0 l$ vertex probability cuts, and the VDET hits requirements. Details on how these efficiency differences between data and Monte Carlo were obtained are presented in appendix B. These investigations show that the efficiency in the Monte Carlo for these cuts is overestimated for both $D^0 \rightarrow K^-\pi^+$ and $D^0 \rightarrow K^-\pi^+\pi^-\pi^+$ decays. To take into account these differences, the reconstruction efficiencies in the $D^0 \rightarrow K^-\pi^+$ and the $D^0 \rightarrow K^-\pi^+\pi^-\pi^+$ decay channels must be downscaled by $(23.0 \pm 5.3)\%$ and $(21.6 \pm 8.4)\%$ respectively.

3 q^2 reconstruction

The reconstruction of the q^2 of the decay $\overline{B}^0 \rightarrow D^{*+} l^- \overline{\nu}_l$ requires access to the 4-momentum of the neutrino, or equivalently to the 4-momentum of the B, which corresponds to three unknowns. The neutrino energy (one constraint) is evaluated in a standard way from the missing energy in the hemisphere. The direction given by the primary vertex and the B decay vertex measures the B flight direction (two constraints) almost independently of the kinematics of the decay. The fourth and most precise constraint is the requirement that the (D^*, l, ν) triplet should have the mass of the B^0. This system is over-constrained and will be solved by the χ^2 minimization described below.

The neutrino 4-momentum is obtained from a MINUIT minimization where two variables are free, the neutrino energy E_ν and the angle ϕ between the neutrino momentum and the vector $\vec{u}_V$ (the unit vector joining the primary to the secondary vertices) projected on a plane orthogonal to $\vec{P}_{D^* l}$.

The B mass constraint imposes:

$$M_B^2 = M_{D^* l}^2 + 2E_{D^* l}E_\nu - 2P_{D^* l}E_\nu \cos\gamma$$

Where γ is the angle between the neutrino and $\vec{P}_{D^* l}$.

Given the orthonormal basis $(\vec{i}, \vec{j}, \vec{k})$ where $\vec{i}$ is colinear to $\vec{P}_{D^* l}$, $\vec{j}$ is in the $(\vec{P}_{D^* l}, \vec{u}_V)$ plane, perpendicular to $\vec{i}$ and oriented towards $\vec{u}_V$:

$$\vec{P}_\nu = E_\nu(\vec{i}\cos\gamma + \vec{j}\sin\gamma\cos\phi + \vec{k}\sin\gamma\sin\phi)$$

[4] In the Monte Carlo simulation (HVFL04), $\tau_{B^0} = 1.5$ ps and $x_B = 0.677$ ($\epsilon_b = 0.006$) while the measured values are $\tau_{B^0} = 1.61$ ps [15] and $x_B = 0.714$ [17] ($\epsilon_b = 0.002$).

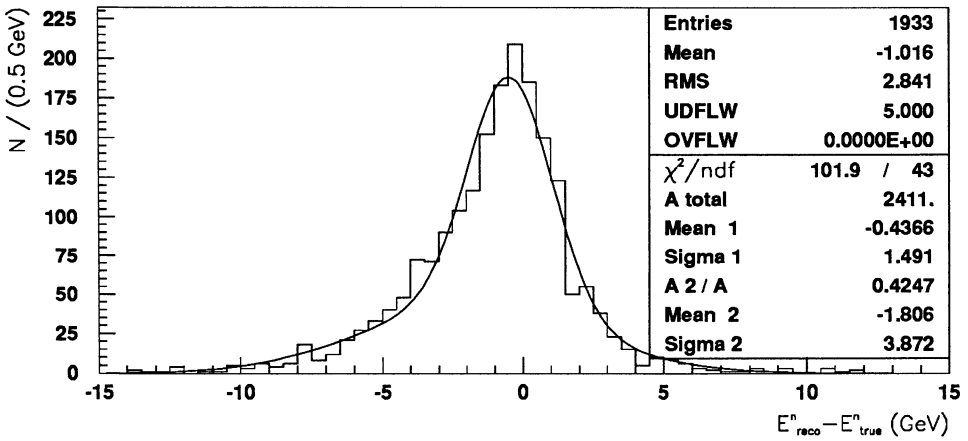

Figure 2: Neutrino energy resolution with the two-gaussian fit used to parametrized it in the q^2 reconstruction fit.

The B momentum is obviously obtained by:

$$\vec{P}_B = \vec{P}_{D^{*}l} + \vec{P}_\nu$$

The χ^2 is made of two parts, one to ensure the constraint on the neutrino energy from the missing energy, the other to constrain on the B direction to the direction given by the vector joining the primary and secondary vertices:

$$\chi^2 = \chi^2_E + \chi^2_V$$

χ^2_E corresponds to a two-gaussian fit of the neutrino energy resolution :

$$\chi^2_E = -2\log\{\frac{1-A_2^{E_\nu}}{\sqrt{2\pi}\sigma_{E_\nu 1}}\exp\frac{(E_\nu - E_\nu^{rec} + E_{\nu 1})^2}{2\sigma^2_{E_\nu 1}} + \frac{A_2^{E_\nu}}{\sqrt{2\pi}\sigma_{E_\nu 2}}\exp\frac{(E_\nu - E_\nu^{rec} + E_{\nu 2})^2}{2\sigma^2_{E_\nu 2}}\} \quad (1)$$

where $E_\nu^{rec} = E_{beam} - E_{vis} + \frac{M^2_{opp} - M^2_{same}}{4E_{beam}}$, E_{vis} is the visible energy in the hemisphere measured with charged, neutral and hadronic residual energy. M_{same} and M_{opp} are the mass of the same and opposite hemisphere [13].

$E_{\nu 1}$, $\sigma_{E_\nu 1}$ are the mean and the sigma of the first gaussian, $A_2^{E_\nu}$ $E_{\nu 2}$, $\sigma_{E_\nu 2}$ are the relative area, the mean and the sigma of the second gaussian used to parametrize the neutrino energy resolution as measured from signal Monte-Carlo (see figure 2).

χ^2_V tells how close is the B direction to the direction given by the vector $\vec{u}_V$, taking into account the error matrices on both vertices [5].

[5]This is the χ^2 of the so-called "most probable decay length" calculated using the routine

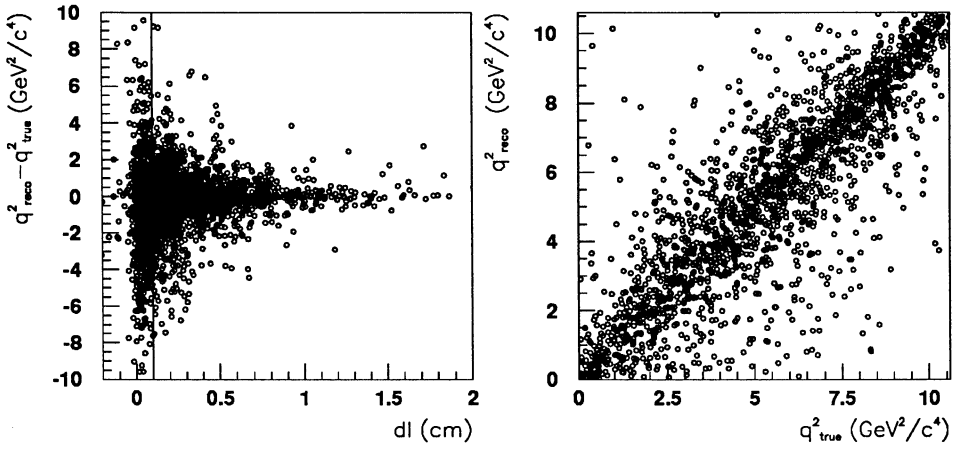

Figure 3: (left) q^2 resolution versus B decay length; the vertical line indicates the 1 mm decay length cut. (right) Reconstructed q^2 versus true q^2 after the decay length cut.

Minimizing the χ^2 with respect to E_ν and ϕ gives access to $\vec{P}_\nu$. q^2 is then easily deduced from $\vec{P}_\nu$ and $\vec{P}_l$. Figure 3 shows the spread of the q^2 resolution as a function of the decay length, justifying the necessity of a cut on the decay length at 1 mm [6]. It displays also the correlation between the reconstructed q^2 and the true q^2. Figure 4 shows the q^2 resolution well fitted with a double gaussian.

4 Background sources and physics background rejection

4.1 Background sources

Besides $\overline{B^0} \to D^{*+} l^- \overline{\nu_l}$, six sources of background contribute to $D^{*+} l^-$ combinations in hadronic Z^0 decays :

1. $B^- \to D^{*+} l^- \overline{\nu_l} \pi^-$
2. $\overline{B^0} \to D^{*+} l^- \overline{\nu_l} \pi^0$

DKLN3D from Robert Johnson and modified by Alan Litke to get the χ^2. It is the minimum of the following χ^2: $\chi^2(\vec{v}_1', \vec{v}_2', l) = (\vec{v}_1' - \vec{v}_1)^T M_1^{-1} (\vec{v}_1' - \vec{v}_1) + (\vec{v}_2' - \vec{v}_2)^T M_2^{-1} (\vec{v}_2' - \vec{v}_2) + \vec{\lambda}^T (l\vec{u}_B - \vec{v}_1' + \vec{v}_2')$ where, v_1 and v_2 are the primary and secondary vertices, M_1 and M_2 the corresponding covariance matrices, $\vec{u}_B$ is the assumed B direction, $\vec{v}_1'$,$\vec{v}_2'$,$\vec{\lambda}$ are free 3-vectors and l is the free decay length.

[6] This cut also reduces combinatorial background and allows efficient $D^{*+} l\nu X$ event rejection.

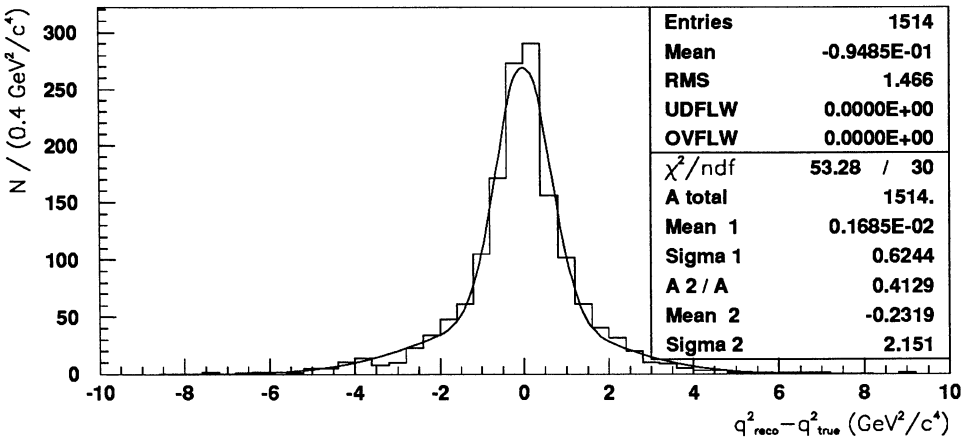

Figure 4: q^2 resolution after all cuts with the double gaussian fit used to parametrized it in the $|V_{cb}|$ fit.

3. $\overline{B_s^0} \to D^{*+} l^- \overline{\nu_l} K^0$
4. $\overline{B^0} \to D^{*+} \tau^- \overline{\nu_\tau}$, $\tau^- \to l^- \overline{\nu_l} \nu_\tau$
5. $\overline{B^0} \to D^{*+} D_s^{(*)-} X$, $D_s^- \to X l^- \overline{\nu_l}$
6. Accidental combinations

To date the branching fractions of the five physics background processes are partially known. Process (1) [7] has recently been measured by ALEPH [8], processes (2), (3) and (4) have not been measured experimentally, while process (5) is poorly known. The branching ratios used in this analysis for these background processes are listed in table 2. Details on how these branching ratios were estimated are presented in appendix A.

Background process	Branching fraction (%)
$B^- \to D^{*+} l^- \overline{\nu_l} \pi^-$	1.00 ± 0.33
$\overline{B^0} \to D^{*+} l^- \overline{\nu_l} \pi^0$	0.50 ± 0.17
$\overline{B_s^0} \to D^{*+} l^- \overline{\nu_l} K^0$	1.00 ± 0.33
$\overline{B^0} \to D^{*+} \tau^- \overline{\nu_\tau}$, $\tau^- \to l^- \overline{\nu_l} \nu_\tau$	0.37 ± 0.06
$\overline{B^0} \to D^{*+} D_s^{(*)-} X$, $D_s^- \to X l^- \overline{\nu_l}$	0.37 ± 0.16

Table 2: Branching fraction of physics background processes used in the analysis.

[7] here we refer to narrow and wide resonant, and non-resonant $D^{*+}\pi^-$ production.

Background process	$N_{D^{*+}l^-}$	
$B^- \to D^{*+} l^- \overline{\nu_l} \pi^-$	390.5 ± 128.9	35.0 ± 11.6
$\overline{B^0} \to D^{*+} l^- \overline{\nu_l} \pi^0$	195.3 ± 66.4	18.4 ± 6.3
$\overline{B_s^0} \to D^{*+} l^- \overline{\nu_l} K^0$	126.6 ± 41.8	11.7 ± 3.9
$\overline{B^0} \to D^{*+} \tau^- \overline{\nu_\tau}$, $\tau^- \to l^- \overline{\nu_l} \nu_\tau$	143.4 ± 23.3	10.1 ± 1.6
$\overline{B^0} \to D^{*+} D_s^{(*)-} X$, $D_s^- \to X l^- \overline{\nu_l}$	143.4 ± 62.0	5.3 ± 2.3
total	1006.9 ± 164.8	80.5 ± 14.1

Table 3: The expected number of $D^{*+}l^-$ events from physics background processes for 1,5 million hadronic Z^0 decays, from branching ratios (first column) and after recontruction with basic cuts (second column). The quoted errors come from errors on the branching ratios.

For 1,5 million hadronic Z^0 decays, the expected numbers of $D^{*+}l^-$ combinations originating from physics background processes before and after reconstruction with basic cuts are listed in table 3.

The accidental combinations are either real/fake lepton in association with fake D^0 (fake D^0 accidentals) or fake lepton in association with real D^0 (fake lepton accidentals). The fake D^0 accidentals lead to a flat D^0 mass distribution under the D^0 mass peak and can be evaluated from the second order polynomial fit, wherease the fake lepton accidentals may contribute to the D^0 mass peak but connot be evaluted from the polynomial fit. To estimate the contribution of fake lepton accidentals in the D^0 mass peak we selected $D^{*+}h^-$ events, where h^- stand for a charged hadron, in the same way as $D^{*+}l^-$ but with lepton selection used in a veto mode. The number of fake lepton accidentals is determined from the selected number of $D^{*+}h^-$ and $D^{*+}l^-$ events, the number of misidentified hadrons, and the probability of lepton misidentification, in the following way:

$$N_{lepton}^{fake} = \left[N_{D^{*+}h^-} - (N_{D^{*+}l^-} \times \frac{1-\epsilon_l}{\epsilon_l}) \right] \times \epsilon_{mis}$$

Where $N_{D^{*+}h^-}$ and $N_{D^{*+}l^-}$ are respectively the selected numbers of $D^{*+}h^-$ and $D^{*+}l^-$ events, ϵ_l the lepton detection efficiency and ϵ_{mis} the probability of hadron mis identification. For the last two parameters we used the following values : $\epsilon_l = 0.85 \pm 0.03$ and $\epsilon_{mis} = 0.01 \pm 0.002$.

The expected number of fake lepton accidentals after basic cuts is 8.0 ± 1.6. Combined with the number of fake D^0 accidentals extracted from the polynomial fit of the D^0 mass distributions (table 1), the expected number of accidentals combinations after basic cuts is 49.6 ± 7.8.

cut	$D^{*+}l^-\nu$	$D^{*+}l^-\nu\pi^-$
$\frac{\delta}{\sigma_\delta} > 3$ or $\frac{\delta}{\sigma_\delta} < -3$	87%	20%
$\frac{\delta}{\sigma_\delta} > 3$ or $\frac{\delta}{\sigma_\delta} < -2$	92%	26%
$\frac{\delta}{\sigma_\delta} > 3$ or $\frac{\delta}{\sigma_\delta} < -1.5$	95%	31%
$\frac{\delta}{\sigma_\delta} > 3$ or $\frac{\delta}{\sigma_\delta} < -1$	97 %	40%

Table 4: Efficiency of the impact parameter cut for signal and physics background $B^- \rightarrow D^{*+}l^-\overline{\nu_l}\pi^-$ events.

4.2 Physics background rejection

Figure 5 shows the q^2 distribution of data and backgrounds after basic cuts. The shape of the background q^2 distribution is smooth but the level of background is clearly high: the total number of $D^{*+}l^-$ events originating from the five physics background processes listed in the previous section is 80.5 events, representing a relative fraction of 22.9% with respect to the total $D^{*+}l^-$ selected pairs (accidental combinations included). This correspond to a purity in $\overline{B^0} \rightarrow D^{*+}l^-\overline{\nu_l}$ of 62.9%. To improve this purity two additional cuts, called in what follows topological cuts, are used to reject physics background $D^{*+}l^-$ events.

Besides accidental combinations, the main contribution of physics background to $D^{*+}l^-$ pairs comes from process (1) in which one additional charged pion is present in the final state. To reduce the number of $D^{*+}l^-$ events from this background process, any $D^{*+}l^-$ pair associated, in the same hemisphere, with an additional pion of momentum above 1 GeV/c [8] , having the same charge as the lepton and at least one VDET hits in $r\phi$ and z coordinates, is rejected if the signed impact parameter [9] of the pion with respect to the $D^{*+}l^-$ reconstructed vertex falls within -2 and 3 standard deviations. Figure 6 shows the signed impact parameter distribution of the closest additional charged pion to the $D^{*+}l^-$ vertex in unit of standard deviation for signal and physics background events. One can notice, as expected, that most of $B^- \rightarrow D^{*+}l^-\overline{\nu_l}\pi^-$ have an impact parameter around zero. On the other hand signal events associated with a pion from fragmentation have mostly negative impact parameter. hence the use of an asymmetric cut on the signed impact parameter avoid rejecting signal events. Table 4 summarizes the efficiency of the impact parameter cut for signal and physics background $B^- \rightarrow D^{*+}l^-\overline{\nu_l}\pi^-$ events.

The second cut used to reject physics background processes is based on the neutrino reconstruction described in section 3. Since we have four constraints for three unknowns, the constraint on the B mass can be relaxed to actually

[8] Lower momentum pions suffer from poor impact parameter resolution; moreover, pions from D^{**} or from 4-body decays are not expected to be particularly soft.

[9] The sign of the impact parameter is given by the cosine of the angle between the $D^{*+}l^-$ direction and the vector pointing from the $D^{*+}l^-$ vertex to the point of closest approach of the pion track.

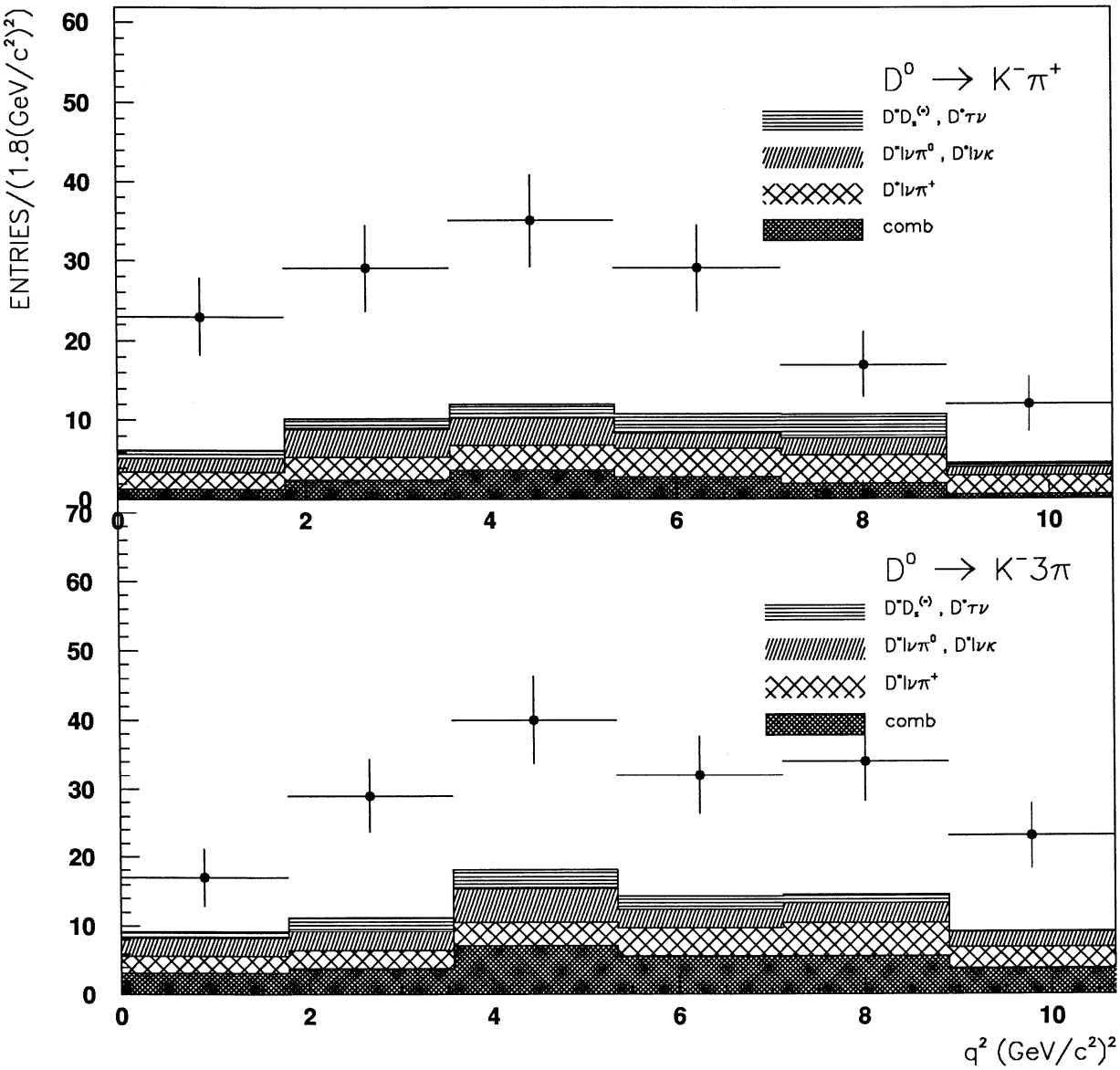

Figure 5: q^2 distribution of $D^{*+}l^-$ candidates after basic cuts and before topological cuts. Points are data, histograms are backgrounds.

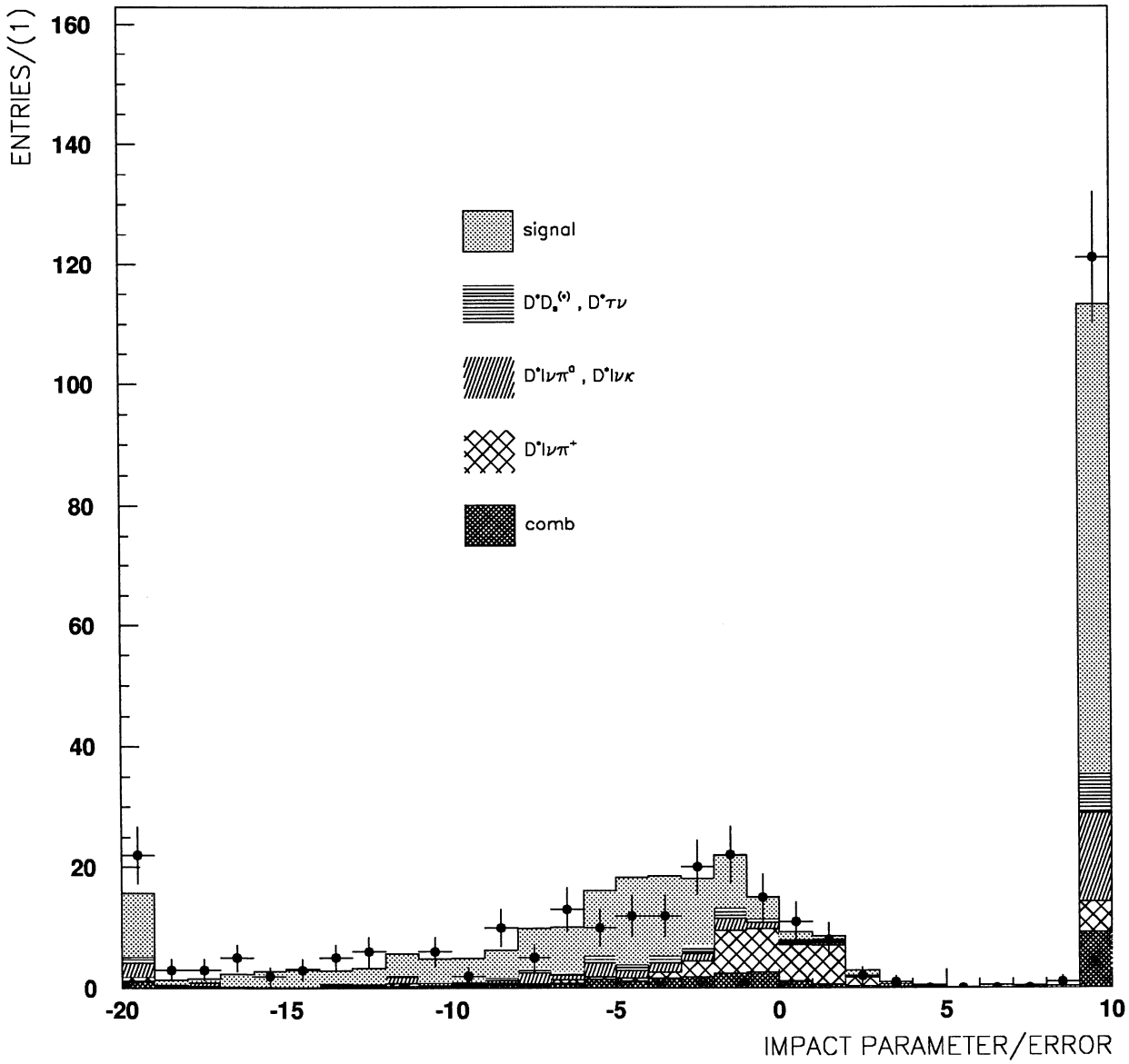

Figure 6: The impact parameter distribution of the closest additional charged pion to the $D^{*+}l^-$ reconstructed vertex in units of standard deviations for signal and background events after basic cuts. The points are data, the solid histograms are Monte Carlo. The area of the signal Monte carlo is adjusted so that the number of events in the Monte Carlo histogram is the same as in data. The rightmost bin corresponds, by convention, to events in which there is no pion with the right charge in the $D^{*+}l^-$ hemisphere. The leftmost bin is an underflow bin.

measure the mass of the $(D^{*+}l^-\nu)$ triplet (refered as M_B^{rec}). The number of constraints is then equal to the number of unknowns; however, the χ^2 fit is still needed when the other constraints are outside allowed values (negative neutrino energy for instance).

Figure 7 shows the reconstructed B mass for signal and background events. Due to the presence of additional particles in the final state, physics background events have a $(D^{*+}l^-\nu)$ invariant mass lower on average than the B mass. Signal events are, as expected, well centered around the B mass. Events with high invariant mass correspond to cases where the reconstructed missing energy is low so that the neutrino direction is poorly defined. It happens in some events that the reconstructed missing energy is negative, in this case the neutrino energy is given the lowest kinematically allowed value.

To reject physics background events, instead of using directly the reconstructed B mass, we define an estimator based on the $\chi^2_{q^2}$ difference of the q^2 fit if the B mass is free or fixed to the true value ($M_B^{true} = 5.279$ GeV/c^2) as follow:

$$\Delta\chi^2 = (\chi^2_{q^2}(M_B = M_B^{true}) - \chi^2_{q^2}(M_B^{rec})) \times sign(M_B^{rec} - M_B^{true})$$

Where $sign(M_B^{rec} - M_B^{true})$ is negative if M_B^{rec} is lower than the true B mass, positive otherwise. $\Delta\chi^2$ gives a confidence level for M_B^{rec} to equal M_B^{true}. For example $\Delta\chi^2 < -1$ would mean that the reconstructed B mass is lower than M_B^{true} with a confidence level corresponding to at least one χ^2 unit *i.e.* one standard deviation.

Figure 8 shows the differential and the integrated $\Delta\chi^2$ distributions for signal and background events. Table 5 summarizes the efficiency of the B mass estimator $\Delta\chi^2$ for signal and physics backgrounds events $\overline{B} \to D^{*+}l^-\overline{\nu}(\pi^-/\pi^0)$.

cut	$D^{*+}l^-\overline{\nu}$	$D^{*+}l^-\overline{\nu}\pi^{-/0}$
$\Delta\chi^2 > -0.5$	80%	59%
$\Delta\chi^2 > -1$	86%	63%
$\Delta\chi^2 > -1.5$	90%	67%
$\Delta\chi^2 > -2$	93%	69%

Table 5: Efficiency of the B mass estimator $\Delta\chi^2$ cut for signal and physics backgrounds events $\overline{B} \to D^{*+}l^-\overline{\nu}(\pi^-/\pi^0)$.

In summary, to reduce physics background events contributions in the $D^{*+}l^-$ final sample, any $D^{*+}l^-$ events having $-2 < \frac{\delta}{\sigma_\delta} < 3$ or $\Delta\chi^2 < -1$ are rejected.

The reconstruction efficiencies for signal and physics background [10] processes

[10]The efficiency of $B^- \to D^{*+}l^-\overline{\nu_l}\pi^-$ is measured on a Monte Carlo sample of 55% resonant $B^- \to D_1^0 l^-\overline{\nu_l}$ and 45% of 4-body decay [8].

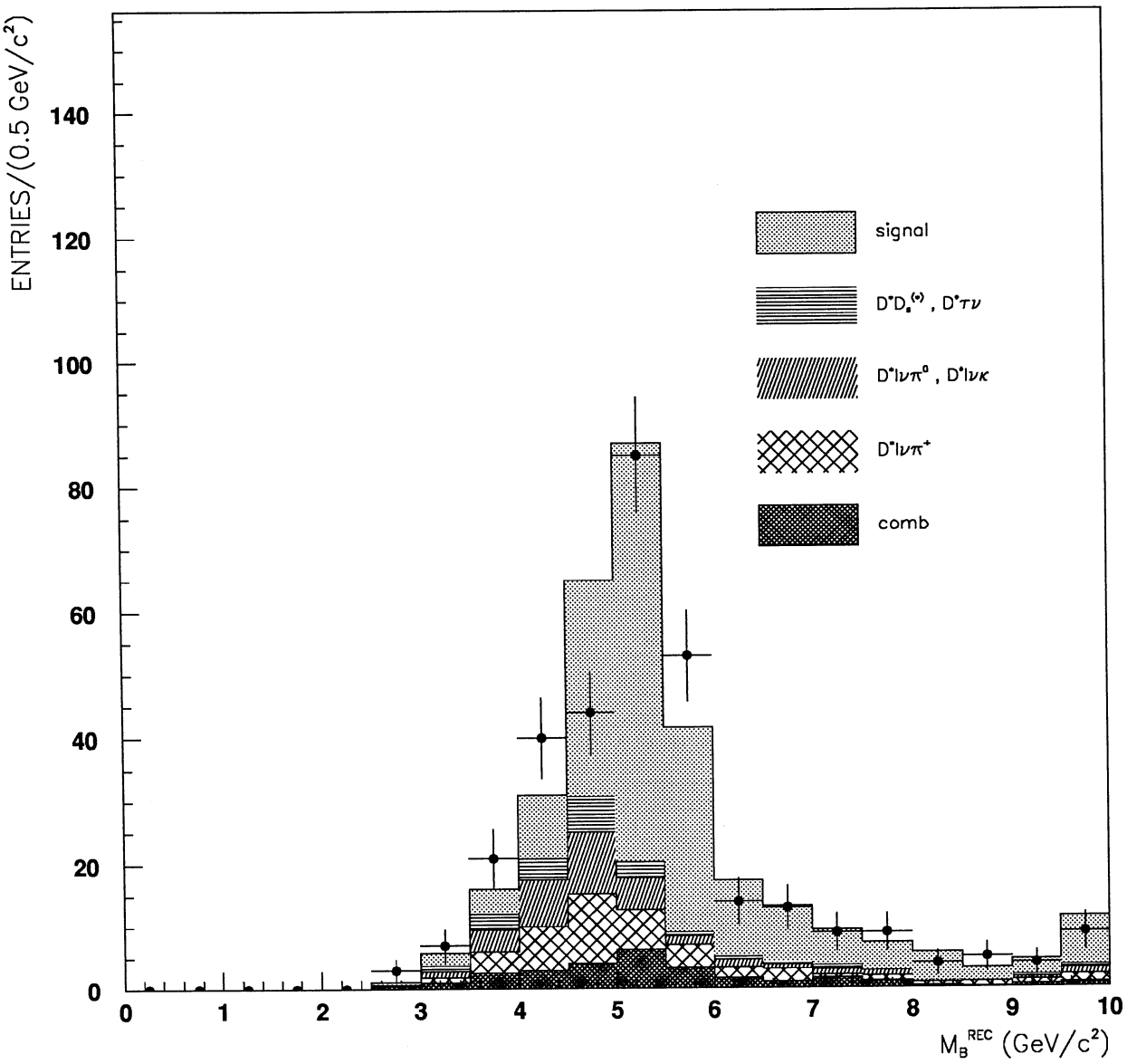

Figure 7: The reconstructed B mass for signal and background events after basic cuts. The points are data, the solid histograms are Monte Carlo.

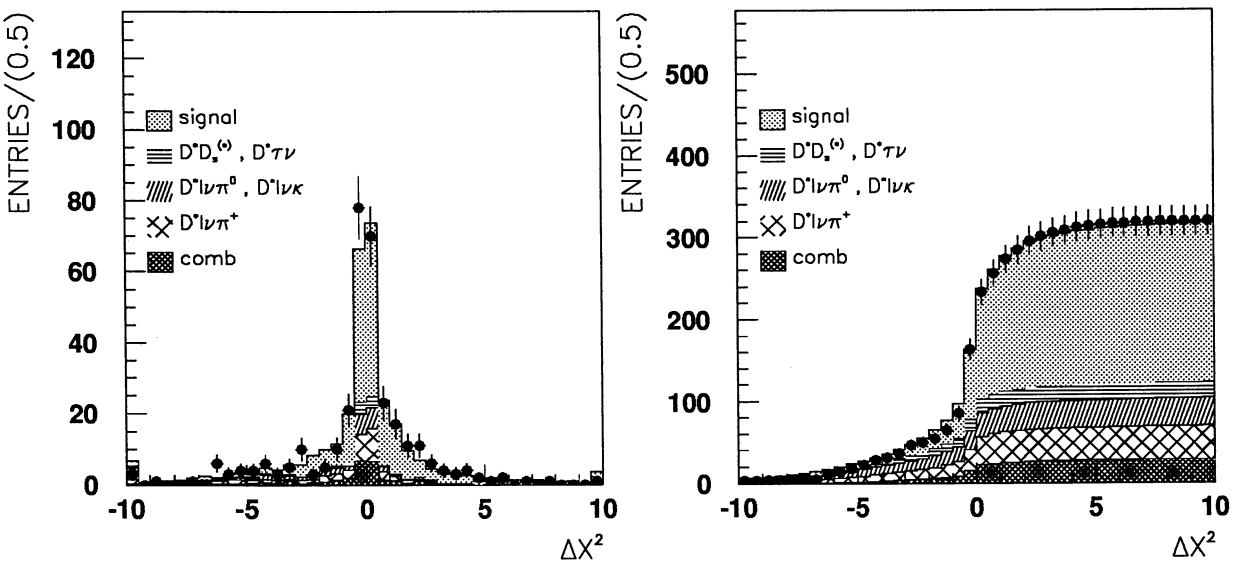

Figure 8: The B mass estimator $\Delta\chi^2$ for signal and background events after basic cuts. The left-hand plot is the differential $\Delta\chi^2$ distribution, the right-hand plot is the integrated $\Delta\chi^2$ distribution. Points are data and the solid histograms are Monte Carlo.

after all cuts and data/MC correction are summarized in table 6. They do not include the D^{*+} and the D^0 branching fractions.

Decay process	detection efficiency (%)	
	$D^0 \to K^-\pi^+\pi^-\pi^+$	$D^0 \to K^-\pi^+$
$\overline{B^0} \to D^{*+}l^-\overline{\nu_l}$	5.61 ± 0.25	10.18 ± 0.36
$B^- \to D^{*+}l^-\overline{\nu_l}\pi^-$	1.36 ± 0.30	1.76 ± 0.33
$\overline{B^0} \to D^{*+}l^-\overline{\nu_l}\pi^0$	4.56 ± 0.68	6.28 ± 0.71
$\overline{B_s^0} \to D^{*+}l^-\overline{\nu_l}K^0$	3.21 ± 1.04	4.09 ± 1.05
$\overline{B^0} \to D^{*+}\tau^-\overline{\nu_\tau}$, $\tau^- \to l^-\overline{\nu_l}\nu_\tau$	2.00 ± 0.47	2.91 ± 0.52
$\overline{B^0} \to D^{*+}D_s^{(*)-}X$, $D_s^- \to Xl^-\overline{\nu_l}$	0.23 ± 0.16	2.05 ± 0.45

Table 6: Reconstruction efficiencies for signal and physics background processes after all cuts and data/MC correction.

Table 7 summarizes the number of $D^{*+}l^-$ events from physics background processes after basic and topological cuts.

Background process	$N_{D^{*+}l^-}$
$B^- \to D^{*+}l^-\overline{\nu_l}\pi^-$	6.1 ± 2.4
$\overline{B^0} \to D^{*+}l^-\overline{\nu_l}\pi^0$	10.2 ± 3.7
$\overline{B_s^0} \to D^{*+}l^-\overline{\nu_l}K^0$	4.5 ± 2.0
$\overline{B^0} \to D^{*+}\tau^-\overline{\nu_\tau}$, $\tau^- \to l^-\overline{\nu_l}\nu_\tau$	3.3 ± 1.5
$\overline{B^0} \to D^{*+}D_s^{(*)-}X$, $D_s^- \to Xl^-\overline{\nu_l}$	1.2 ± 1.0
total	25.3 ± 5.2

Table 7: The expected number of $D^{*+}l^-$ events within 2.5 $\sigma_{M_{D^0}}$ from background processes for 1,5 million hadronic Z^0 decays, after basic and topological cuts. The errors come from uncertainties on the branching ratios and the efficiencies.

Figure 9 shows the invariant mass distributions of the $D^0 \to K^-\pi^+$ and the $D^0 \to K^-\pi^+\pi^-\pi^+$ for opposite-sign $D^{*+}l^-$ and like-sign $D^{*+}l^+$ selected events after basic and topological cuts. To avoid double counting problem, if an event enters more than once in the histogram (mass window 1.8-2.1 GeV/c^2), only the better [11] reconstructed one is kept. This problem happens only in the $D^0 \to K^-\pi^+\pi^-\pi^+$ channel in which K^-/π^- ambiguity leads to different D^0 mass

[11]The following criteria are used to choose between two or more candidates for the same event: candidate with the highest number of VDET hits or the best D^0 vertex or the best D^0l vertex or with a kaon having the best dE/dx value is selected. If after these selection criteria, applied in this order, more than one candidate is left, the selected candidate is then choosen randomly.

Decay process	$N_{D^{*+}l^-}$	fake D^0 accidentals	fake lepton accidentals
$D^0 \rightarrow K^-\pi^+\pi^-\pi^+$	123.0 ± 11.1	8.9 ± 3.6	1.7 ± 0.4
$D^0 \rightarrow K^-\pi^+$	90.0 ± 9.5	4.6 ± 2.6	2.4 ± 0.5
total	213.0 ± 14.6	13.5 ± 4.4	4.1 ± 0.6

Table 8: The number of $D^{*+}l^-$ events within 2.5 $\sigma_{M_{D^0}}$ (accidentals included), fake D^0 and fake lepton accidentals after basic and topological cuts.

values for the same event [12]

The number of $D^{*+}l^-$ candidates and the number of accidental combinations are extracted, within 2.5 sigma of the D^0 mass, from a fit to the two mass distributions from opposite-sign $D^{*+}l^-$ events, with a gaussian representing the D^0 signal and a second order polynomial for fake D^0 accidentals. Table 8 summarizes the results of the fits.

After all cuts, the purity of the final sample in $\overline{B^0} \rightarrow D^{*+}l^-\overline{\nu_l}$ is now 80.0%.

5 $|V_{cb}|$ measurement

The previous sections described the q^2 reconstruction and the careful backgrounds and efficiency estimation which are needed. This section is devoted to the extraction of $|V_{cb}|$ from the selected $D^{*+}l^-$ events.

5.1 Fitting method

The q^2 distributions of the $D^{*+}l^-$ events selected within 2.5 $\sigma_{M_{D^0}}$ have all background contributions subtracted in the following way:

The fake D^0 combinatorial background is taken from data events having D^0 mass between 1.9 and 2.1 GeV/c^2 (see figure 9). The left-hand side band cannot be used because of the contamination by genuine D meson with one missing particle. The D^0 candidate is assigned the true D^0 mass before q^2 reconstruction so that the side-band q^2 distribution is the same as the one below the peak.

The fake lepton contribution is taken from inclusive $D^{*+}h^-$ events as described in section 4.1.

The physics background q^2 distributions are taken from dedicated Monte-Carlo events, with number of events as given in table 7. Figure 10 shows the q^2 distribution of data and backgrounds, after all cuts. The shape of the back-

[12]This double counting rejection reduces signal and physics background events by 7.4% and combinatorial background by 16.4%.

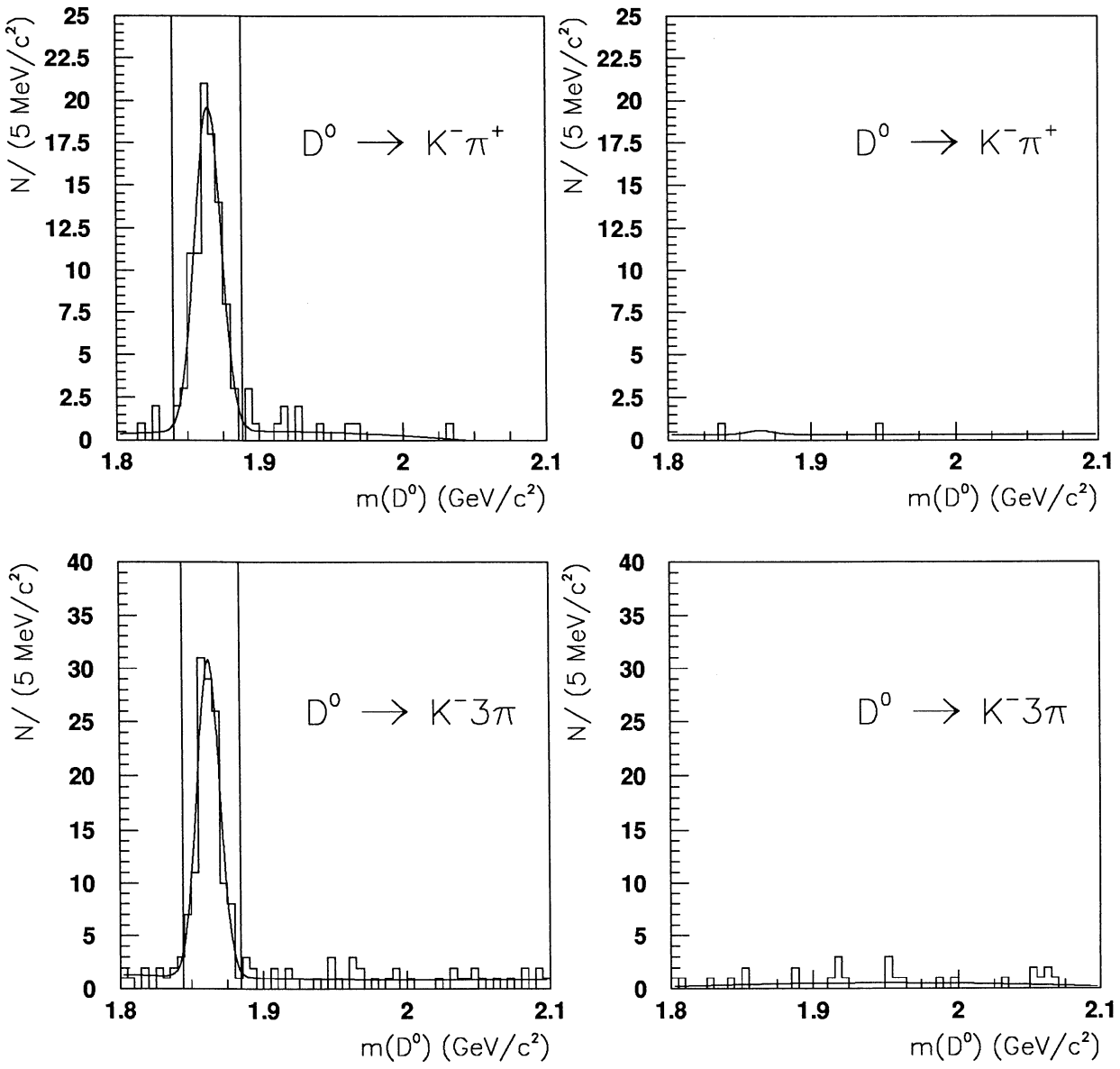

Figure 9: Invariant mass distributions of $D^0 \rightarrow K^-\pi^+$ candidates and $D^0 \rightarrow K^-\pi^+\pi^-\pi^+$ candidates for opposite-sign $D^{*+}l^-$ and like-sign $D^{*+}l^+$ selected events after basic and topological cuts.

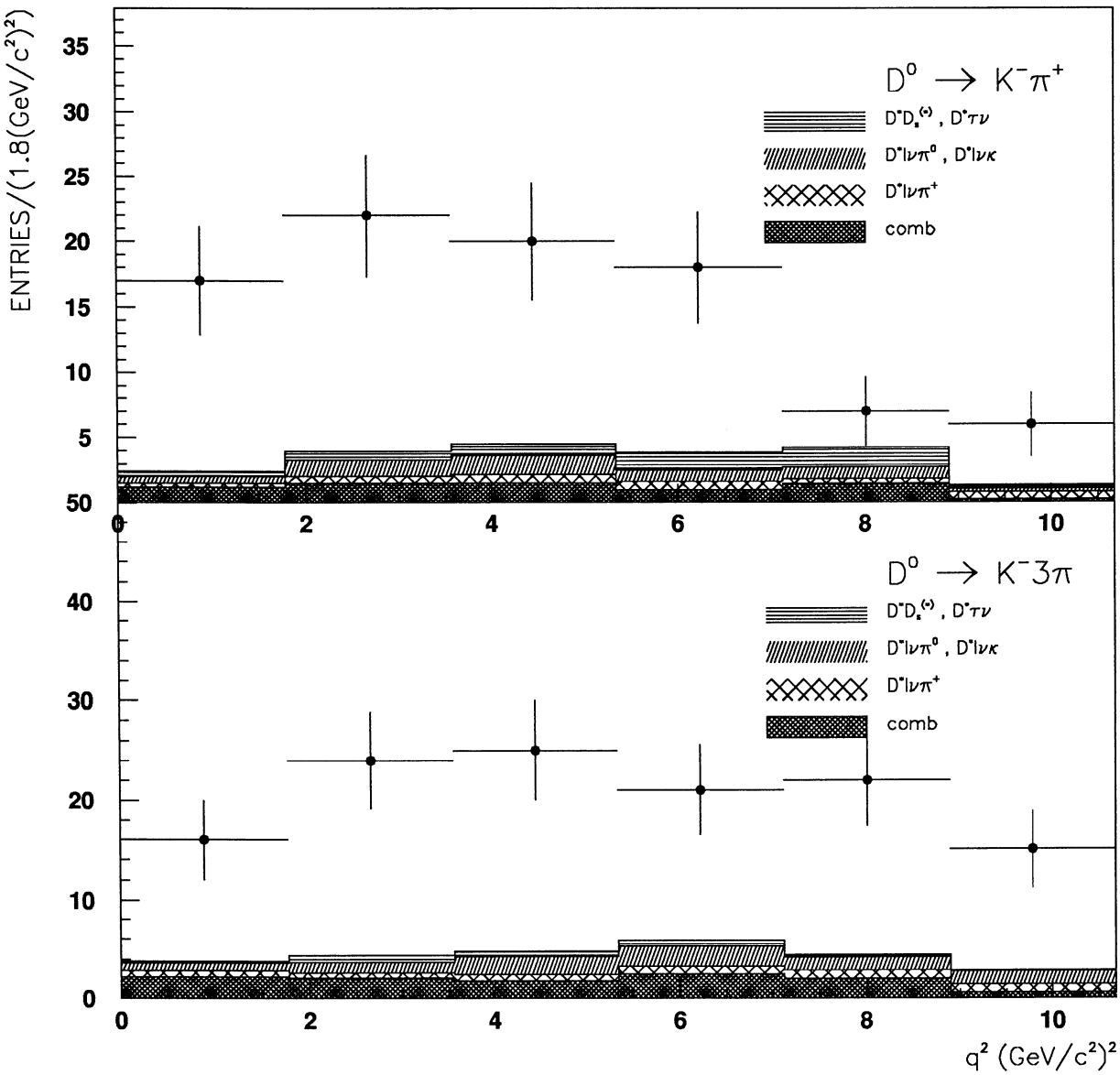

Figure 10: q^2 distribution of $D^{*+}l^-$ candidates after all cuts. Points are data, histograms are backgrounds.

branching ratio	value	reference
$\frac{\Gamma_{b\bar{b}}}{\Gamma_{had}}$	0.2193 ± 0.0029	[10]
$Br(b \to B^0)$	$37 \pm 3\%$	[9]
$Br(D^{*+} \to D^0\pi^+)$	$68.1 \pm 1.3\%$	[11]
$Br(D^0 \to K^-\pi^+)$	$4.01 \pm 0.14\%$	[11]
$\frac{Br(D^0 \to K^-\pi^+\pi^-\pi^+)}{Br(D^0 \to K^-\pi^+)}$	2.02 ± 0.11	[11]

Table 9: Branching ratios used in the physics function. The quoted errors will be used for the estimation of systematics uncertainties.

grounds q^2 distributions (if compared to figure 5) is not affected by the topological cuts but their level is significatively reduced.

The physics function which describes the q^2 distribution of the final $D^{*+}l^-$ sample after background subtraction is the following:

$$\Phi(q^2) = 2N_{q\bar{q}}\frac{\Gamma_{b\bar{b}}}{\Gamma_{had}}Br(b \to B^0)Br(D^* \to D^0\pi^+)Br(D^0 \to Kn\pi)\frac{\tau_B^0}{\hbar}\frac{d\Gamma}{dq^2}(q^2)\epsilon_n(q^2)$$

Where $Br(D^0 \to Kn\pi)$ is the branching ratio of the D^0 decay ($K\pi$ or $K3\pi$); its value and that of the other relevant branching ratios are given in table 9. $\epsilon_n(q^2)$ is the q^2 dependent efficiency of the decay considered parametrized by a second order polynomial:

$$\epsilon_n(q^2) = e_n^0 + e_n^1(q^2 - \frac{q^2_{max}}{2}) + e_n^2(q^2 - \frac{q^2_{max}}{2})^2$$

The differential partial width $\frac{d\Gamma}{dq^2}(q^2)$ is given below [18]:

$$\frac{d\Gamma}{dq^2}(q^2) = \frac{1}{2M_B M_{D^*}}\frac{G_F^2 M_{D^*}^3 (M_B - M_{D^*})^2}{48\pi^3} \times \sqrt{y^2-1}\left(4y(y+1)\frac{(1-2yr+r^2)}{(1-r)^2} + (y+1)^2\right)\left(\eta_A\hat{\xi}(1)|V_{cb}|\right)^2$$

with: $y = \frac{M_B^2 + M_{D^*}^2 - q^2}{2M_B M_{D^*}}$, $r = \frac{M_{D^*}}{M_B}$, η_A contains the QCD perturbative correction and $\hat{\xi}(y)$ is the Isgur-Wise function [13].

The Isgur-Wise function is parametrized by a linear shape ($\hat{\rho}^2$ is a free parameter, so-called "charge radius"):

$$\hat{\xi}(y) = 1 - \hat{\rho}^2(y-1)$$

[13]The symbol "$\cdot$" specifies that the three non-zero form factors are assumed to be equal, which is not rigorously valid away from q^2_{max} (see [18] for detailed explanation).

channel	e^0	e^1	e^2	$\chi^2(n_{dof}=3)$
$D^0 \to K^-\pi^+$	0.113 $\pm$ 0.005	$-0.0025\pm$ 0.0010	$-0.0015\pm$ 0.0004	0.73
$D^0 \to K^-\pi^+\pi^-\pi^+$	0.060 $\pm$ 0.003	$-0.0007\pm$ 0.0007	$-0.0004\pm$ 0.0003	2.09

Table 10: Parameters of the q^2 dependent fit of the efficiency for the two D^0 channels.

The q^2 resolution function R is the sum of two gaussians fitted on the q^2 resolution for each bin of reconstructed q^2. The parameters are displayed in figure 4 for the whole q^2 range. The fitting function used is the convolution of the physics and resolution functions. As by construction, the measured q^2 is constrained to be in the physical domain $0 < q^2 < q^2_{max} = (M_B - M_{D^*})^2$, the resolution function must be renormalised to unit area on the physical domain, or equivalently the convolution written as:

$$F(q^2) = \frac{\int_0^{q^2_{max}} \Phi(q^2) R(q^2_{true} - q^2) dq^2_{true}}{\int_0^{q^2_{max}} R(q^2_{true} - q^2) dq^2_{true}}$$

The q^2 histograms corresponding to the two D^0 decay modes are fitted simultaneously with an binned maximum likelihood method.

5.2 Efficiency fit

The efficiency $\epsilon_n(q^2)$ is obtained from a fit of efficiency histograms obtained from a total of 15,000 generated Monte-Carlo events [14]. and corrected for the fragmentation function, the B^0 lifetime and the other data versus Monte-Carlo correction discussed in appendix B.

The parameters resulting from the fit are shown in table 10 and the corresponding plots are shown in figure 11. The efficiency depends only slightly on the q^2, in contrast with $\Upsilon(4S)$ experiments where the efficiency drops severely at high q^2 due to the misreconstruction of the soft pion. The possible dependence, which seems smaller in the $D^0 \to K^-\pi^+\pi^-\pi^+$ channel, is investigated in appendix D.

5.3 Results

The physics parameters values extracted from the q^2 histograms fit are the following (where the errors are statistical only):

$$\hat{\rho}^2 = 0.16 \pm 0.36(stat)$$

[14] Only the q^2 from the truth is used to build this histogram since the smearing is taken into account by the resolution function.

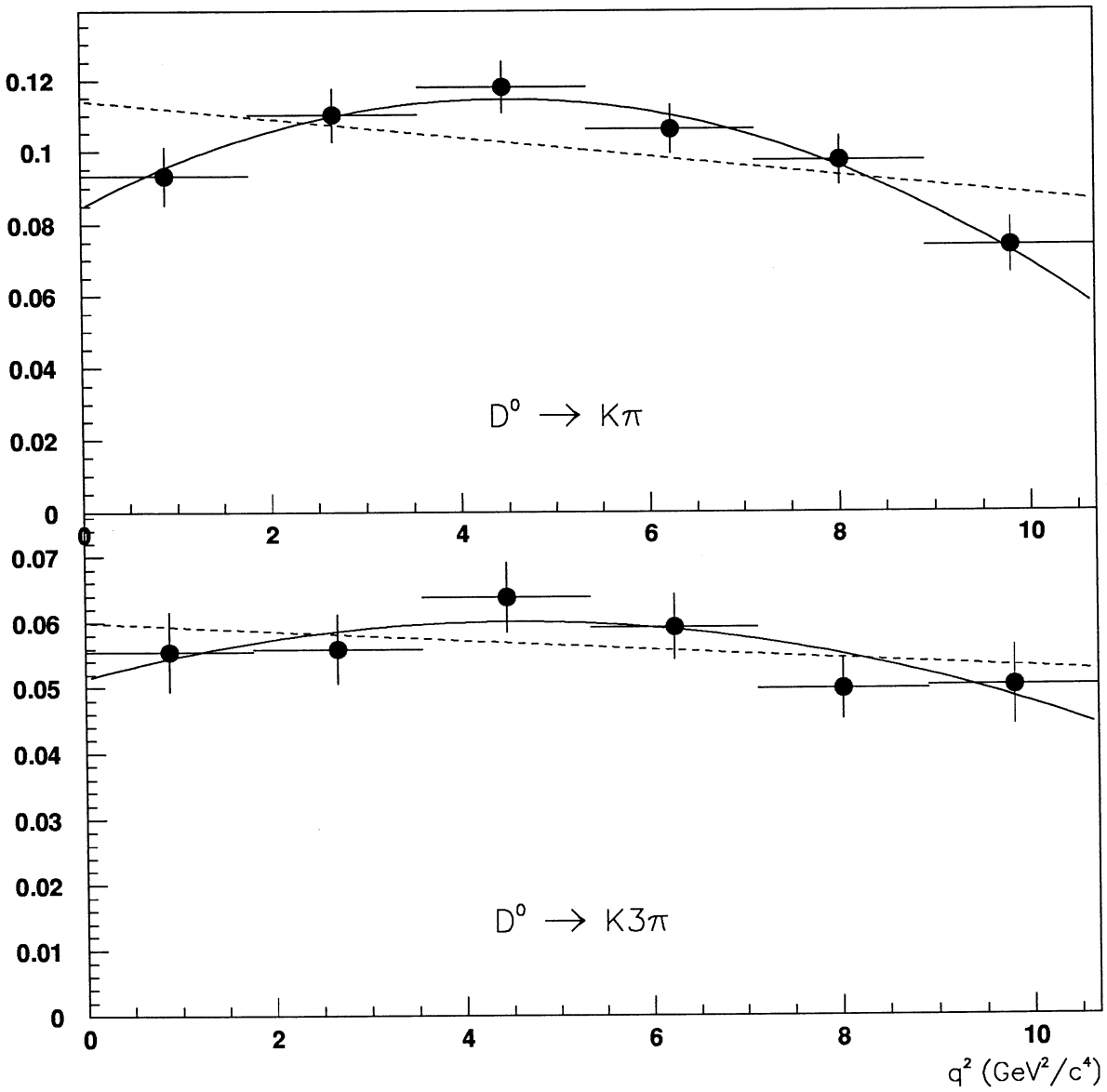

Figure 11: Efficiency as a function of q^2. The solid line is the quadratic fit, the dashed line is the linear fit.

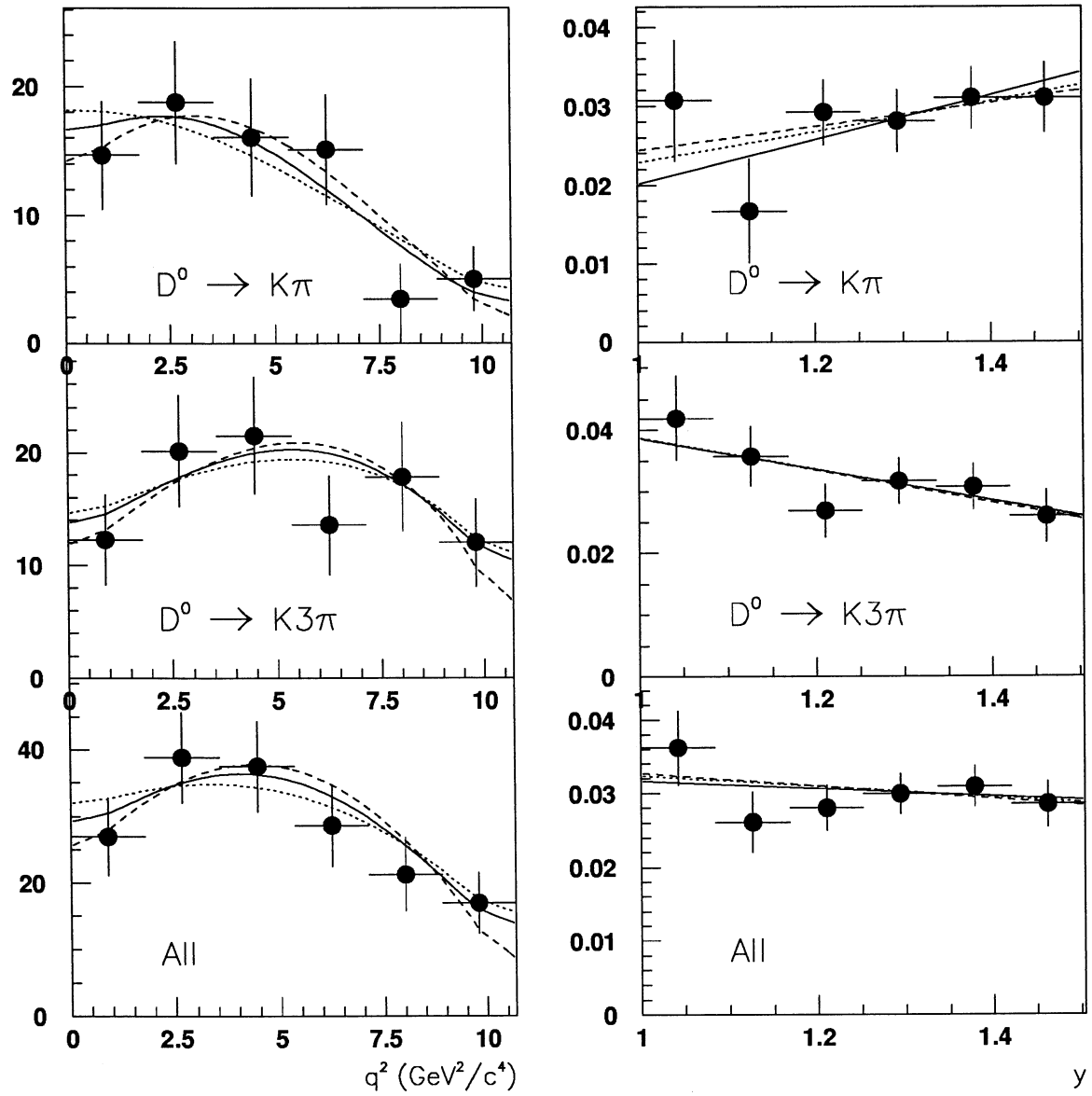

Figure 12: The left column displays q^2 histograms after background subtraction with the fit superimposed for the $D^0 \to K^-\pi^+$ channel, the $D^0 \to K^-\pi^+\pi^-\pi^+$ channel and the sum of the two. The solid lines are the standard fits; the dashed lines are the fits with no q^2 smearing; the dotted lines are the fits with a linear shape of the efficiency. The right column shows the corresponding histogram with the variable y, corrected from efficiency, phase space factor and branching ratios, so that only the shape of the Isgur-Wise function remains;$\eta_A\hat{\xi}(1)|V_{cb}|$is the intercept of the line with the vertical axis at $y = 1$.

channel	$\eta_A\hat{\xi}(1)\lvert V_{cb}\rvert$	$\hat{\rho}^2$	χ^2	Br
$D^0\rightarrow K^-\pi^+$	0.0201 ± 0.0061	-1.40 ± 1.38	2.36/4	$5.44 \pm 0.75\%$
$D^0\rightarrow K^-\pi^+\pi^-\pi^+$	0.0388 ± 0.0045	0.68 ± 0.30	2.69/4	$6.61 \pm 0.80\%$
electron	0.0294 ± 0.0054	-0.14 ± 0.62	5.55/10	$6.19 \pm 0.80\%$
muon	0.0342 ± 0.0053	0.50 ± 0.44	8.06/10	$6.01 \pm 0.77\%$
global	0.0316 ± 0.0037	0.16 ± 0.36	8.60/10	$6.09 \pm 0.56\%$

Table 11: Results of the $|V_{cb}|$ fit for various subsamples and for the global sample.

$$\eta_A\hat{\xi}(1)|V_{cb}| = 0.0316 \pm 0.0037(stat)$$

These two parameters are 93 % correlated. The area of the fitting function is directly related to the branching ratio:

$$Br(\overline{B^0}\rightarrow D^{*+}l^-\bar{\nu}) = 6.09 \pm 0.56(stat)$$

Fitting separately the two channels or events with an electron or a muon give the results shown in table 11. The fits are displayed in figure 12. The value of $\eta_A\hat{\xi}(1)|V_{cb}|$ extracted from the two channels differs by 2.5 standard deviation. This is due to a conjunction of a 1.1 standard deviation discrepancy in the number of observed events (as seen from the branching ratio) and a 1.5 standard deviation discrepancy in the shape of the q^2 distribution. The first discrepancy could come from the $D^0\rightarrow K^-\pi^+$ and $D^0\rightarrow K^-\pi^+\pi^-\pi^+$ branching ratios, while the second one is already visible before physics background subtraction in figure 5 and is not considered significant statistically.

6 Systematics and checks

Various sources of systematics have been considered. Their respective contribution are summarized in table 12; they are described in more detail below. Since $|V_{cb}|$ is proportionnal to the square root of the branching ratio $Br(\overline{B^0}\rightarrow D^{*+}l^-\bar{\nu})$, it will be half less sensitive than the branching ratio to quantities like branching ratio and absolute efficiencies, provided the slope $\hat{\rho}^2$ is unaffected.

Physics background

The contribution of each physics background was varied within errors given in the table 2. As the contribution of the $\overline{B}\rightarrow D^{*+}l^-\nu_l X$ events are proportionnal to ALEPH measurement, the corresponding errors must be added linearly. However, the B_s part suffers also from the uncertainty on $Br(b\rightarrow B_s)$ which is uncorrelated to the other. The total corresponding systematic is 4.2% on $|V_{cb}|$ and 4.1% on the branching ratio.

source	ΔV_{cb} %	$\Delta\hat{\rho}^2$	ΔBr %
$B\to D^* l\nu\pi^+$	1.1	0.02	1.2
$B\to D^* l\nu\pi^0$	1.8	0.03	1.9
$B\to D^* l\nu K^0$	1.8	0.04	1.3
subtotal	4.2	0.08	4.1
$D^*\pi$ (non)resonance	1.9	0.03	2.0
$B\to D^* D_s^{(*)}$	<0.1	<0.01	0.2
$B\to D^*\tau\nu_\tau$	< 0.1	<0.01	0.5
combinatorial background	0.8	< 0.01	1.7
double counting	0.6	0.01	1.0
$Br(b\to B^0)$	3.8	<0.01	8.1
$Br(D^0\to K^-\pi^+)$	1.8	<0.01	3.6
$Br(D^0\to K^-\pi^+)/Br(D^0\to K^-3\pi)$	1.7	<0.01	3.4
Other Br. ratios	1.2	<0.01	2.4
fragmentation	1.5	0.02	3.2
B^0 lifetime	3.3	<0.01	1.5
lepton ID	2.0	0.01	3.0
data *vs* MC efficiency	3.9	0.03	7.1
q^2 smearing	1.7	0.05	-
efficiency shape	2.4	0.06	<1
MC stat. (signal)	2.8	0.09	3.2
total	10.4	0.16	15.6

Table 12: Systematics

channel	quadratic fit	linear fit
$D^0 \to K^-\pi^+$	4.6 ± 1.5	5.3 ± 1.5
$D^0 \to K^-\pi^+\pi^-\pi^+$	8.9 ± 2.0	8.7 ± 1.9

Table 13: Variation on the expected number of background events with the fitting function.

channel	from truth	from fit
$D^0 \to K^-\pi^+$	4	6.4 ± 2.9
$D^0 \to K^-\pi^+\pi^-\pi^+$	42	35.9 ± 7.0

Table 14: Comparison between the real and fitted number of background events in 4 millions $q\bar{q}$ Monte-Carlo events.

Moreover, the fraction of resonant decay in the Monte-Carlo simulation was varied between 0 and 100 % (with a central value of 55%) to account for the lack of knowledge of the non-resonant part. This causes an additionnal uncertainty of 1.9% on $|V_{cb}|$ and 2.0 % on the branching ratio.

Combinatorial background

The combinatorial background below the peak was estimated with a fit of the right-hand side band with a second-order polynomial. The use of a linear fit changes slightly the background estimation as shown in table 7; the change is however negligible compared to the statistical error on the fit.

The procedure of combinatorial background was checked on about 4 million $q\bar{q}$ Monte-Carlo events. After all cuts, the number of background events in the truth is statistically compatible with the fitted number (see table 14). Finally for the estimation of systematics, the number of background events in the $D^0 \to K^-\pi^+$ and $D^0 \to K^-\pi^+\pi^-\pi^+$ samples is taken to be 4.6 ± 1.5 and 8.9 ± 2.0 respectively, which correspond to a change of $|V_{cb}|$ of 0.8% and 1.5 % of the branching ratio.

Double counting

The method used to suppress double-entries in the $D^0 \to K^-\pi^+\pi^-\pi^+$ channel (best candidate in the wide $1.8 - 2.1 \mathrm{GeV/c^2}$ mass window, chosen with mass unrelated criterion) is not unique. As a conservative upper limit on the systematic error on the choice of the method, the number of combinatorial events is varied to its value before double entries rejection which is 11.6 ± 2.2, giving a systematic of 0.6% on $|V_{cb}|$ and 1.0 % on the branching ratio.

Branching ratios

The physics function Φ is proportional to the branching ratios listed in table 9 with their errors; they affect also the expected number of physics back-

Cut	$D^0 \to K^-\pi^+$	$D^0 \to K^-3\pi$
Pi soft P_t, (P_K)	$0.6 \pm 0.1\%$	$2.5 \pm 0.1\%$
P lepton	$1.1 \pm 0.1\%$	$1.2 \pm 0.1\%$
reconstruction	$1.1 \pm 0.3\%$	$-0.2 \pm 0.3\%$
VDET hits	$-2.3 \pm 0.2\%$	$-0.5 \pm 0.2\%$
D^0 vertex	$-0.8 \pm 0.1\%$	$2.1 \pm 0.4\%$
$D^0 l$ vertex	$0.7 \pm 0.1\%$	$0.0 \pm 0.2\%$
B decay-length	$1.8 \pm 0.3\%$	$1.1 \pm 0.5\%$
$\Delta\chi^2$	$-0.9 \pm 0.2\%$	$0.0 \pm 0.3\%$
topological pion	$2.2 \pm 0.2\%$	$2.1 \pm 0.3\%$
total	$3.2 \pm 0.9\%$	$9.0 \pm 1.0\%$

Table 15: Correction on the efficiency of the main cuts due to change of ϵ_B from 0.006 to 0.002. The error is the statistical error of the reweighting procedure.

ground events. The dominant systematic is from $Br(b \to B^0)$ which is taken from ALEPH paper on B^0 mixing. The fact that the branching ratio of $D^0 \to K^-\pi^+\pi^-\pi^+$ is normalised to the one of $D^0 \to K^-\pi^+$ is taken into account.

Fragmentation

The mean B hadron momentum has been measured by ALEPH to be : $x_B = 0.714 \pm 0.012$ [17], which corresponds to $\epsilon_B = 0.002^{+0.001}_{-0.0008}$. The Monte-Carlo events have been reweigthed with the Peterson function according to the z_B parameter as available in the FZFR bank. This caused an increase of the efficiency of $3.2 \pm 1.4\%$ for the $D^0 \to K^-\pi^+$ channel and $9.0 \pm 3.0\%$ for the the $D^0 \to K^-\pi^+\pi^-\pi^+$ channel (see table 15 for details). The uncertainty comes from the uncertainty on ϵ_B and also from the statistical uncertainty on the reweighting of the events (weights up to 5 have to be used). It corresponds to a systematic error of 1.5 % on $|V_{cb}|$ and 3.2 % on the branching ratio [15].

B^0 lifetime

A change in B^0 lifetime affects $|V_{cb}|$ in two ways. An increase in the lifetime will directly decrease the partial width for the same branching ratio. But, the branching ratio will also decrease because the cut on the decay length at 1 mm and also the additionnal background rejection cuts favour long lifetime events. The use of $\tau_{B^0} = 1.61 \pm 0.08$ ps resulted in an increase of the efficiency of $1.9 \pm 1.4\%$, and a decrease of the branching ratio of $2.0 \pm 1.5\%$. The net uncertainty is 3.3% on $|V_{cb}|$ and 1.5 % on the branching ratio.

A change in the B^+ and B_s lifetimes within errors also affects the proportion of physics background but this has a negligible effect on the final results.

Lepton identification

[15]The impact on the branching ratio is more important than the impact on the efficiency, because the number of physics background events is also affected.

After data vs Monte-carlo correction, the uncertainty on the lepton efficiency is taken to be 3%.

The fake lepton mis-identification probability (electron plus muon) was taken to be $1.0 \pm 0.2\%$, the uncertainty taking into account the not quite standard electron identification and also the electron from conversion. The corresponding uncertainties are 0.2% on $|V_{cb}|$ and 0.5% on the branching ratio, negligible compared to the uncertainty on the lepton efficiency.

Data *vs* Monte-Carlo efficiency correction

The data *vs* Monte-Carlo efficiency ratio of the dE/dx, VDET hits, vertices probability was evaluated in section 2.2. The error on this ratio (5.3% for $D^0 \rightarrow K^-\pi^+$, 8.4% for $D^0 \rightarrow K^-\pi^+\pi^-\pi^+$) propagates into a systematic of 3.9% on $|V_{cb}|$ and 7.1% on the branching ratio. The fact that the final sample is included in the one used to calculate the efficiency correction introduces a positive correlation between the efficiency correction factor and the final number of events. However, since the measured branching ratio is proportionnal to the number of events divided by the corrective factor, it is conservative not to take this correlation into account in the propagation of the error. Finally, it should be noted that this systematic error is in fact of statistical nature.

Neutrino energy reconstruction

Changing the parametrization of the q^2 resolution to the one obtained after an arbitrary shift of 2 GeV (which is an extremely conservative estimate of the absolute calibration of the energy flow) in the neutrino resolution change the results by a negligible amount. The efficiency is also little affected (by less than 3 %).

However, checks of the neutrino energy performed in appendix C show that the residual hadronic energy is not adequately simulated. To take this into account, the analysis has been redone without using the residual hadronic energy. The neutrino energy resolution is then shifted by +1.7GeV (compared to -0.9 GeV before); this shift is taken out by the neutrino resolution in equation 1 in section 3. The branching ratio then decreases by 4% because of a different behaviour of the $\Delta\chi^2$ cut. The slope $\hat{\rho}^2$ decreases from 0.16 to 0.01 and $|V_{cb}|$ decreases by 9%. This sensitivity to the use of the neutral hadronic energy is somehow contradictory with the unsensitivity to a global shift; it will be investigated in the future.

Smearing The accuracy of the resolution function is not crucial. In fact, if the fit is performed without any q^2 smearing the value of $|V_{cb}|$ changes by 3.4%. The systematic on the smearing is taken to be half of this value. It means that we do not need to worry about getting the q^2 resolution from Monte-Carlo and about the fact that the q^2 resolution depends of the B decay length or momentum.

Efficiency shape

If the fit is redone with a linear (instead of quadratic) shape of the efficiency

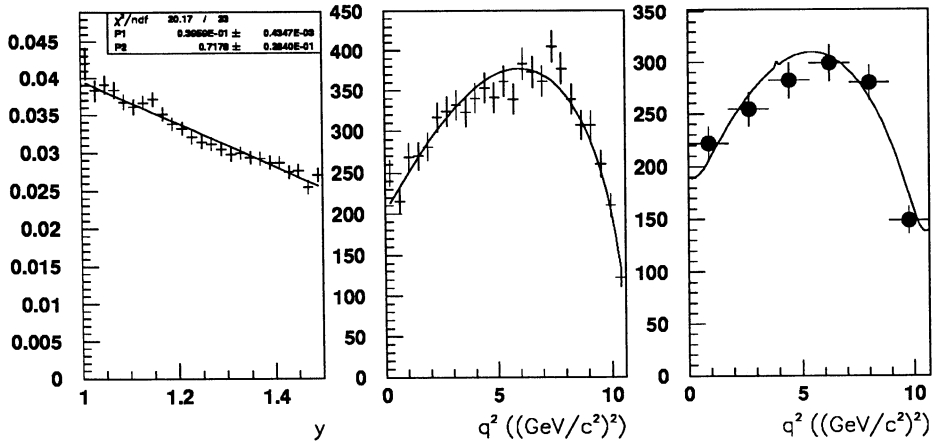

Figure 13: (left) y distribution from 15,000 generated signal Monte-Carlo events corrected so that only the Isgur-Wise function shape appears. (middle) The raw true q^2 distribution with the drawing of the expected shape with the fit parameters from the left hand side histogram. (right) The reconstructed q^2 histogram with the smeared function fit for the reconstructed events.

as a function of q^2, $\hat{\rho}^2$ is increased by .05 corresponding to a change in $|V_{cb}|$ of 2.4 % which is considered to be the corresponding systematics.

Check of fitting procedure

The semi-leptonic decay model (Körner-Schüler) used in the Monte-Carlo is such that the y distribution fits very well (after phase space correction) with an Isgur-Wise function being linear with a slope of 0.76 ± 0.02 (see figure 13). A fit of the reconstructed q^2 histogram from 15,000 Monte-Carlo signal events gives a slope of 0.73 ± 0.08. A fit of the reconstructed q^2 histogram from 4 million Monte-Carlo $q\bar{q}$ events gives a slope of 0.67 ± 0.12 showing the absence of any significant bias from the reconstruction and fitting method.

Choice of the Isgur-Wise parametrization

Our result is taken from a linear fit of the q^2 distribution, however the Isgur-Wise function is basically unknown. Besides the linear parameterization, we have tried others found in the litterature [19]. Table 16 shows the very small dependence of the results on the parameterization. This is due to the fact that the fitted value of $\hat{\rho}^2$ is small and that the whole y range is small rendering all functions nearly linear.

Summary

Combining the systematic errors from the different sources in quadrature, the total systematic error is : 10.4% for $|V_{cb}|$ and 15.6% for $\overline{B^0} \to D^{*+} l^- \overline{\nu_l}$ branching fraction.

$\hat{\xi}(y)$ parameterization	$\eta_A\hat{\xi}(1)\lvert V_{cb}\rvert$	$\hat{\rho}^2$	$\chi^2(n_{dof}=10)$
$1-\hat{\rho}^2(y-1)$	0.0316 ± 0.0037	0.16 ± 0.36	8.60
$\exp(-\hat{\rho}^2(y-1))$	0.0316 ± 0.0038	0.17 ± 0.40	8.60
$\frac{1+y}{2}^{-2\hat{\rho}^2}$	0.0317 ± 0.0040	0.19 ± 0.45	8.60
$\frac{2}{y+1}\exp\left((1-2\hat{\rho}^2)\frac{y-1}{y+1}\right)$	0.0316 ± 0.0041	0.15 ± 0.51	8.60

Table 16: Comparison between different Isgur-Wise function parameterizations.

7 Conclusion

From a data sample of 1,5 million hadronic Z^0 decays collected with the ALEPH detector in 1991, 1992 and 1993, we have measured :

$$Br(\overline{B^0}\rightarrow D^{*+}l^-\overline{\nu_l}) = 6.09 \pm 0.56(stat.) \pm 0.95(syst.)\%$$

$$\eta_A\hat{\xi}(1)|V_{cb}| = 0.0316 \pm 0.0037(stat.) \pm 0.0033(syst.)\%.$$

$$\hat{\rho}^2 = 0.16 \pm 0.36(stat.) \pm 0.16(syst.)$$

Assuming $\eta_A\hat{\xi}(1) = 0.93 \pm 0.03$ [18] :

$$|V_{cb}| = 0.0333 \pm 0.0040(stat.) \pm 0.0035(syst.) \pm 0.0011(theory)$$

These results have to be compared with CLEO's [5] contribution at the Glasgow Conference:

$$\eta_A\hat{\xi}(1)|V_{cb}| = 0.0347 \pm 0.0019(stat.) \pm 0.0020(syst.)\%.$$

and with ALEPH's [6] contribution at the Glasgow Conference

$$\eta_A\hat{\xi}(1)|V_{cb}| = 0.0382 \pm 0.0044(stat.) \pm 0.0035(syst.)\%.$$

and with the latest theoretical estimation of the slope[18]:

$$\hat{\rho}^2 = 0.7 \pm 0.2$$

A Branching fractions of physics background

Physics background processes listed in section 2.2 have not been all measured. To estimate their branching fractions we use, whenever available the measured values, and evaluate the unmeasured processes by analogy with known decays.

Process $B^- \to D^{*+} l^- \overline{\nu_l} \pi^-$ has been measured recently by ALEPH [8] in term of product branching ratios :

$$Br(b \to B^-) \times Br(B^- \to D^{*+} \pi^- l^- \overline{\nu_l} X) = (3.7 \pm 1.0_{stat} \pm 0.7_{syst})\ 10^{-3}$$

Using the measured branching ratio [16] $Br(b \to B^0) = 0.37 \pm 0.03$ from ref. [9], the branching fraction of process $B^- \to D^{*+} l^- \overline{\nu_l} \pi^-$ is :

$$Br(B^- \to D^{*+} l^- \overline{\nu_l} \pi^-) = (1.00 \pm 0.33)\% \tag{2}$$

From isospin considerations process $\overline{B^0} \to D^{*+} l^- \overline{\nu_l} \pi^0$ is expected to be produced with a half rate of process $B^- \to D^{*+} l^- \overline{\nu_l} \pi^-$.

To estimate the branching fraction of process $\overline{B_s^0} \to D^{*+} l^- \overline{\nu_l} K^0$ we suppose that its decay rate is similar to process $B^- \to D^{*+} l^- \overline{\nu_l} \pi^-$. Hence we use :

$$Br(\overline{B_s^0} \to D^{*+} l^- \overline{\nu_l} K^0) = Br(B^- \to D^{*+} l^- \overline{\nu_l} \pi^-)$$

In conclusion, the branching fraction used for processes $B^- \to D^{*+} l^- \overline{\nu_l} \pi^-$ and $\overline{B_s^0} \to D^{*+} l^- \overline{\nu_l} K^0$ are :

$$Br(\overline{B^0} \to D^{*+} l^- \overline{\nu_l} \pi^0) = (0.50 \pm 0.17)\% \tag{3}$$
$$Br(\overline{B_s^0} \to D^{*+} l^- \overline{\nu_l} K^0) = (1.00 \pm 0.33)\% \tag{4}$$

The B_s production rate $Br(b \to B_s)$ is taken to be $12 \pm 4\%$, as in [14].

The branching fraction of process $\overline{B^0} \to D^{*+} \tau^- \overline{\nu_\tau}$ can be estimated from the inclusive $b \to X \tau^- \nu_\tau$ branching ratio. From spin arguments we expect $Br(\overline{B^0} \to D^{*+} \tau^- \overline{\nu_\tau})$ to be at most $3/4 \times Br(b \to X \tau^- \nu_\tau)$. Using $Br(b \to X \tau^- \nu_\tau) = (2.75 \pm 0.30 \pm 0.37)\%$ measured by ALEPH [12], we find [17] :

$$Br(\overline{B^0} \to D^{*+} \tau^- \overline{\nu_\tau}) = (2.06 \pm 0.36)\% \tag{5}$$

The branching fraction of process $\overline{B^0} \to D^{*+} D_s^{(*)-} X$ has already been measured at lower energy machines [7] ($Br(\overline{B^0} \to D^{*+} D_s^{(*)-} X) = (4.3 \pm 1.1 \pm 0.5)\%$)

[16] Here we assume that $Br(b \to B^0) = Br(b \to B^-)$.

[17] For our analysis, this value has to be downscaled by $Br(\tau^- \to l^- \overline{\nu_l} \nu_\tau) = (17.83 \pm 0.21)\%$ ref. [7].

but $Br(D_s^- \to Xl^-\overline{\nu_l})$ is partially known. If we suppose that $\Gamma^{sl}_{D_s^-} = \Gamma^{sl}_{D^-}$, the branching fraction of $D_s^- \to Xl^-\overline{\nu_l}$, where l^- stands for either an electron or a muon, can be evaluated in the following way :

$$Br(D_s^- \to Xl^-\overline{\nu_l}) = \frac{Br(D^- \to Xl^-\overline{\nu_l})}{\tau_{D^-}} \times \tau_{D_s^-} = (7.6 \pm 0.9)\%$$

For $D_s^- \to \tau^-\nu_\tau$, the branching fraction has not been measured. It can be estimated from the theoretical expressions of $\Gamma(D_s^- \to \mu^-\nu_\mu)$, $\Gamma(D_s^- \to \tau^-\nu_\tau)$, and the measured [7] $Br(D_s^- \to \mu^-\nu_\mu) = (0.59 \pm 0.22)\%$:

$$Br(D_s^- \to \tau^-\nu_\tau) = Br(D_s^- \to \mu^-\nu_\mu) \times \frac{m_\tau^2(m_{D_s}^2 - m_\tau^2)}{m_\mu^2(m_{D_s}^2 - m_\mu^2)} = (5.75 \pm 2.14)\%$$

As for process (4) $Br(D_s^- \to \tau^-\nu_\tau)$ has to be downscaled by $Br(\tau^- \to l^-\overline{\nu_l}\nu_\tau)$.

Adding all contributions, $Br(\overline{B^0} \to D^{*+}D_s^{(*)-}X) \times Br(D_s^- \to Xl^-\overline{\nu_l})$ is estimated to be :

$$Br(\overline{B^0} \to D^{*+}D_s^{(*)-}X) \times Br(D_s^- \to Xl^-\overline{\nu_l}) = (3.7 \pm 1.6)\ 10^{-3} \qquad (6)$$

B Recontruction efficiency: Data versus Monte Carlo

Among the set of cuts used to select $D^{*+}l^-$ events, the dE/dx cut, the D^0 and D^0l vertex probability cuts, and the VDET hits requirements may lead to different efficiencies in data and Monte Carlo. To estimate the magnitude of this difference, these cuts were applied on two Monte Carlo samples (signal and general $q\bar{q}$ Monte Carlo) and the corresponding efficiencies were compared to those obtained from real data. Tables 17 summarize the efficiency differences between data and Monte Carlo for $D^0 \to K^-\pi^+$ and $D^0 \to K^-\pi^+\pi^-\pi^+$. As one can notice the efficiency values in the two Monte Carlo samples agree very well. Compared to data these values presents a significant difference due mainly to the D^0 probability cut. This difference does not depend on the D^0 momentum as shown in figures 14 and 15.

An other difference between data and Monte Carlo is due to lepton detection efficiency and has also to be taken into account. This difference [20] is equal to $(97.0 \pm 3.0)\%$.

In conclusion the reconstruction efficiency estimated from the Monte Carlo has to be down scaled by $(23.0 \pm 5.3)\%$ for $D^0 \to K^-\pi^+$ and by $(21.6 \pm 8.4)\%$ for $D^0 \to K^-\pi^+\pi^-\pi^+$.

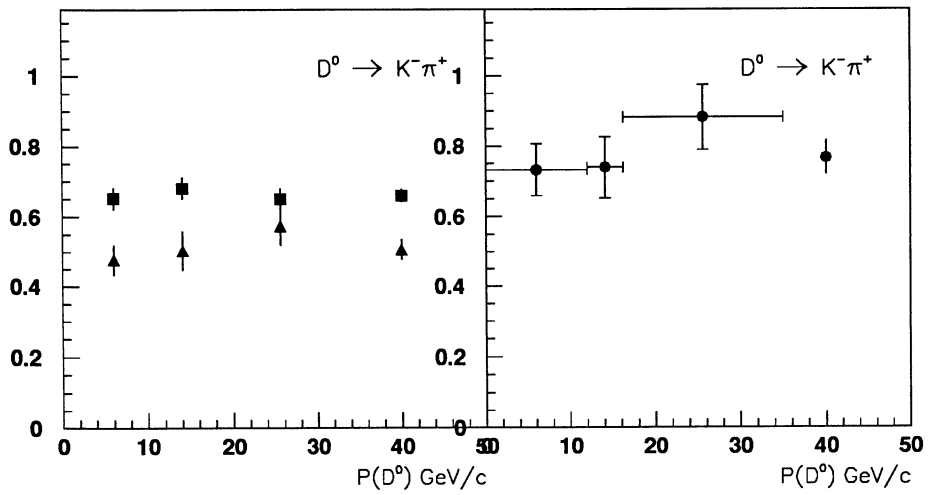

Figure 14: Dependence of the efficiency with D^0 momentum for the VDET hit requirement and D^0 and $D^0 l$ vertex cuts for the $D^0 \rightarrow K^-\pi^+$channel. On the left plot, the squares are Monte-Carlo $q\bar{q}$ efficiencies, the triangles are data efficiencies. On the right plot, the points are data over Monte-Carlo efficiencies ratio; the horizontal error bars indicate the width of the three bins in D^0 momentum chosen to be approximately equally populated . The rightmost points are the average over the whole spectrum.

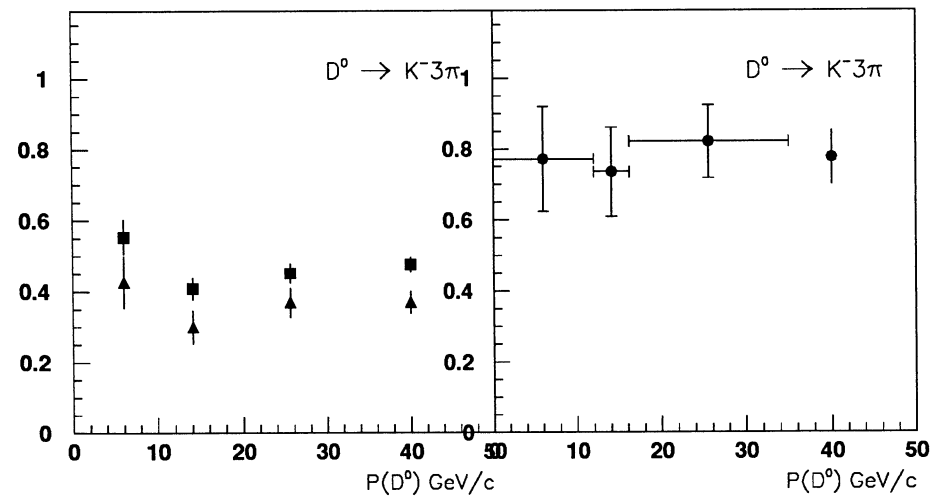

Figure 15: Dependence of the efficiency with D^0 momentum for the VDET hit requirement and D^0 and $D^0 l$ vertex cuts for the $D^0 \rightarrow K^-\pi^+\pi^-\pi^+$ channel. See caption of figure 14 for details.

$D^0 \rightarrow K^-\pi^+$	Signal MC(%)	$q\bar{q}$ MC(%)	Data (%)	Data/$q\bar{q}$ (%)
dE/dx	96.3 ± 0.3	96.2 ± 1.5	97.1 ± 1.7	1.01 ± 0.03
VDET hits (D^0)	84.7 ± 0.7	86.0 ± 1.5	79.6 ± 2.7	92.3 ± 3.4
VDET hits (lepton)	91.8 ± 0.5	92.0 ± 1.0	88.4 ± 2.1	96.0 ± 2.3
Prob(D^0)	91.1 ± 0.6	93.3 ± 1.3	83.5 ± 2.7	89.4 ± 3.0
Prob($D^0 l$)	92.3 ± 0.6	89.4 ± 1.4	85.0 ± 2.9	95.0 ± 3.4
Total	63.1 ± 0.9	63.8 ± 2.1	49.1 ± 3.0	77.0 ± 5.3

$D^0 \rightarrow K^-\pi^+\pi^-\pi^+$	Signal MC(%)	$q\bar{q}$ MC(%)	Data (%)	Data/$q\bar{q}$ (%)
dE/dx	96.0 ± 0.4	96.2 ± 1.5	97.1 ± 1.7	1.01 ± 0.03
VDET hits (D^0)	95.6 ± 0.4	96.6 ± 0.9	94.7 ± 2.1	98.0 ± 2.1
VDET hits (lepton)	91.5 ± 0.5	89.5 ± 1.5	88.2 ± 2.8	98.5 ± 3.4
Prob(D^0)	63.1 ± 1.0	60.6 ± 2.7	49.3 ± 4.3	81.3 ± 6.3
Prob($D^0 l$)	90.6 ± 0.8	90.1 ± 1.8	89.0 ± 3.6	98.7 ± 4.3
Total	48.2 ± 1.0	45.8 ± 2.3	35.9 ± 3.4	78.4 ± 8.4

Table 17: Comparison of efficiencies between data and Monte Carlo for dE/dx, VDET hits and vertex cuts. The efficiency value quoted for each cut is computed with respect to the previous one.

C Check of the neutrino energy reconstruction

Once the neutrino 4-momentum is reconstructed, we have access to any variable related to the B center of mass. The cosine of the decay angle of the neutrino ($\cos\theta^*_\nu$) is particularly interesting because its distribution should be flat, it is not really affected by the kinematic cuts applied (in contrast with $\cos\theta^*_l$) and will be affected directly by any bias in the neutrino energy. Figure 16 shows the comparison on this variable between data and Monte-Carlo. The combinatorial background is clearly peaked at -1, corresponding to an underestimation of the missing energy in the B decay. The agreement between data and Monte-Carlo is only reasonable. The amount of neutral and charged energy in the $D^{*+}l^-$ hemisphere were compared in data versus Monte-Carlo. The only clear disagreement appears with the hadronic energy, as shown figure 17 . To take this into account the analysis was repeated without using the hadronic energy to estimate the systematics error related to missing energy reconstruction.

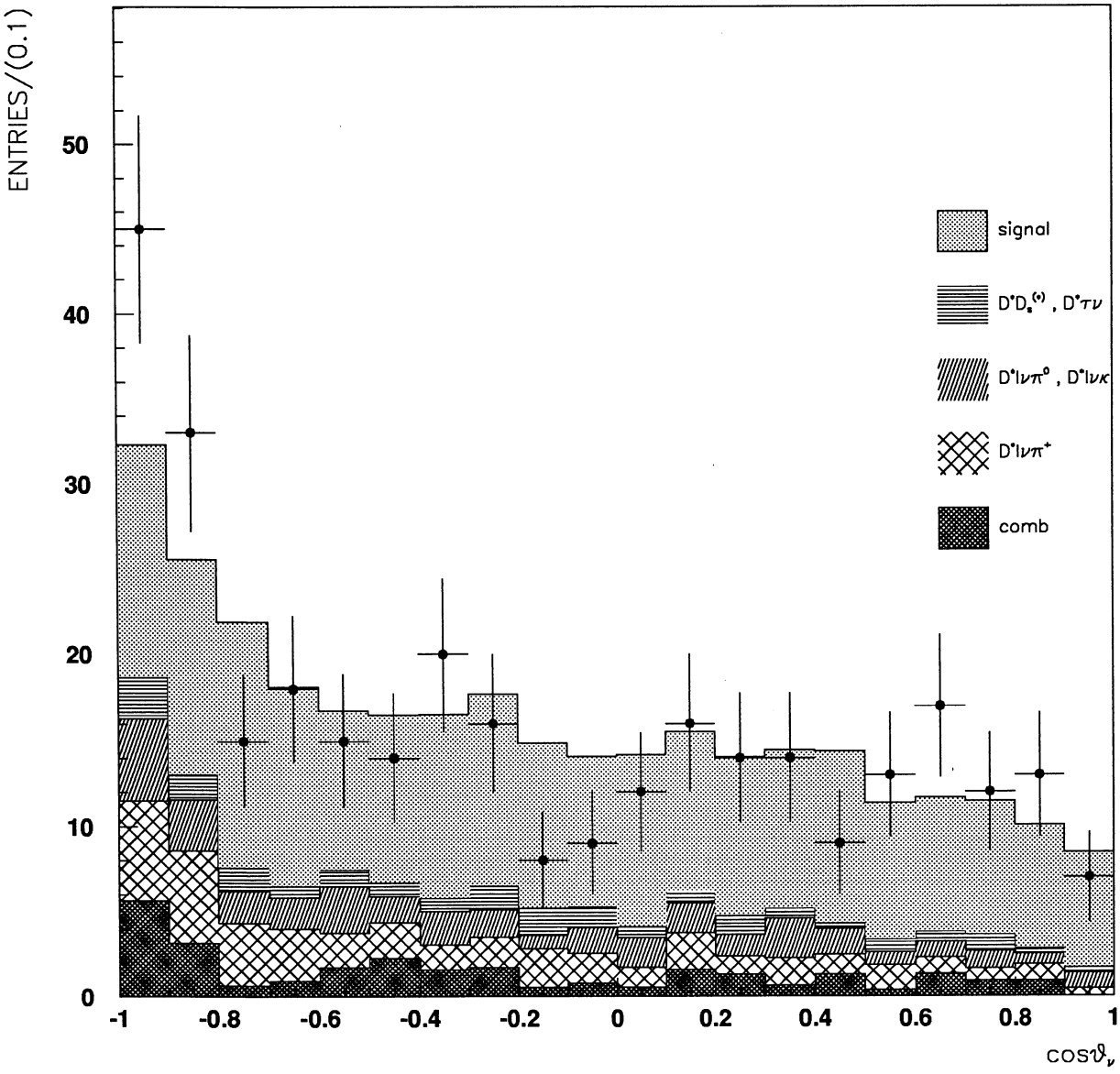

Figure 16: Decay angle of the neutrino in the B rest frame

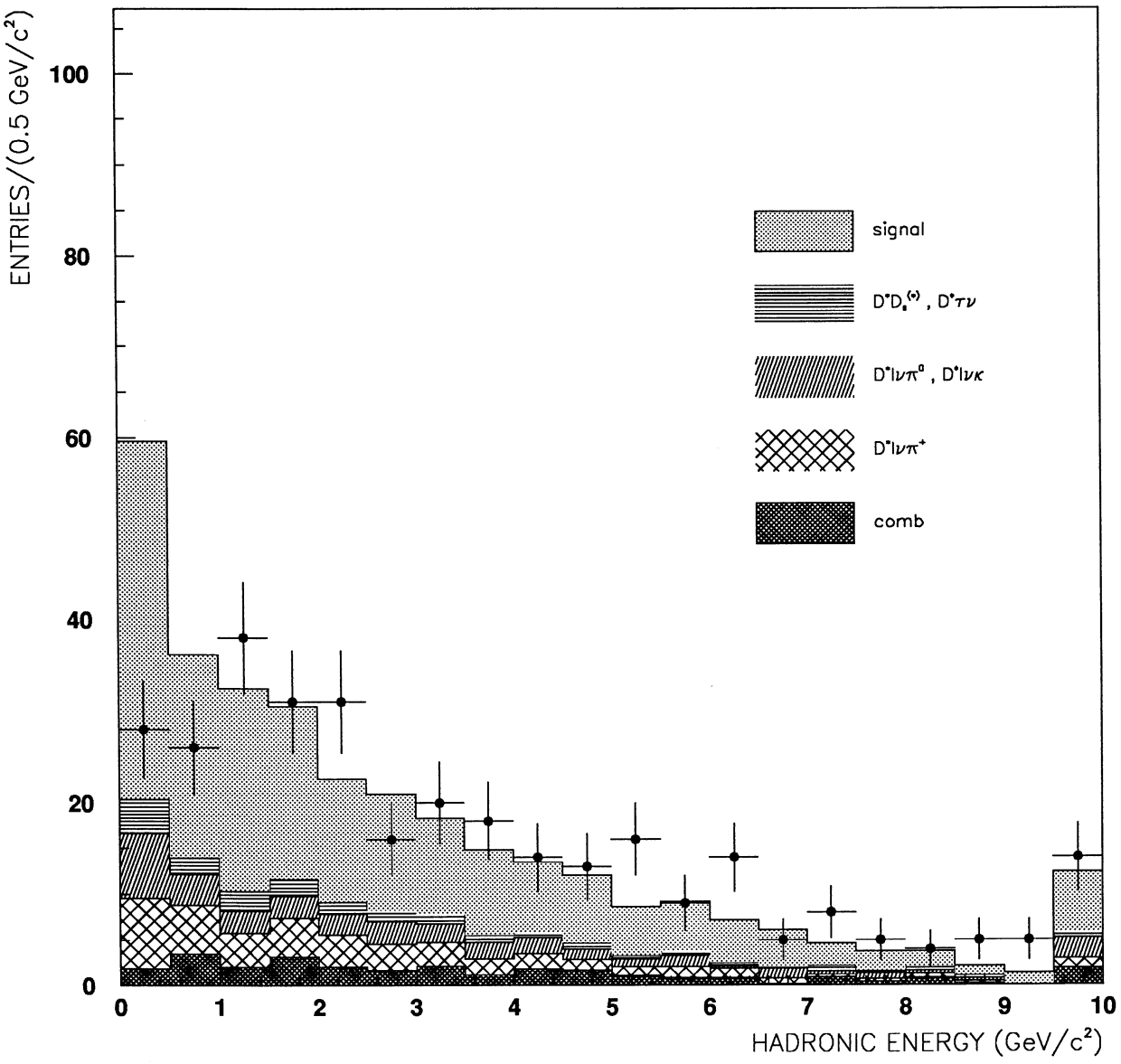

Figure 17: Residual hadronic energy in the hemisphere of the $D^{*+}l^-$ candidate

D q^2 dependence of efficiency

We have investigated which cut has a q^2 dependence by plotting the shape of the efficiency for each cut (see figure 18 and 19, the total efficiency is shown on figure 11).

The cuts which are the most q^2 dependent are the cuts on the lepton momentum and the cut on $\Delta\chi^2$. The leftmost and right most bins seem also affected by the reconstruction stage in the $D^0 \to K^-\pi^+$ channel (i.e particle identification and solid angle cuts). The origin of the parabolic shape of the efficiency in the $D^0 \to K^-\pi^+$ channel is due to the combination of the cuts. However since it is unclear why it does not appear also in the $D^0 \to K^-\pi^+\pi^-\pi^+$ channel a systematic will be attributed to it by quoting the difference between the linear fit and the quadratic fit (sea table 12).

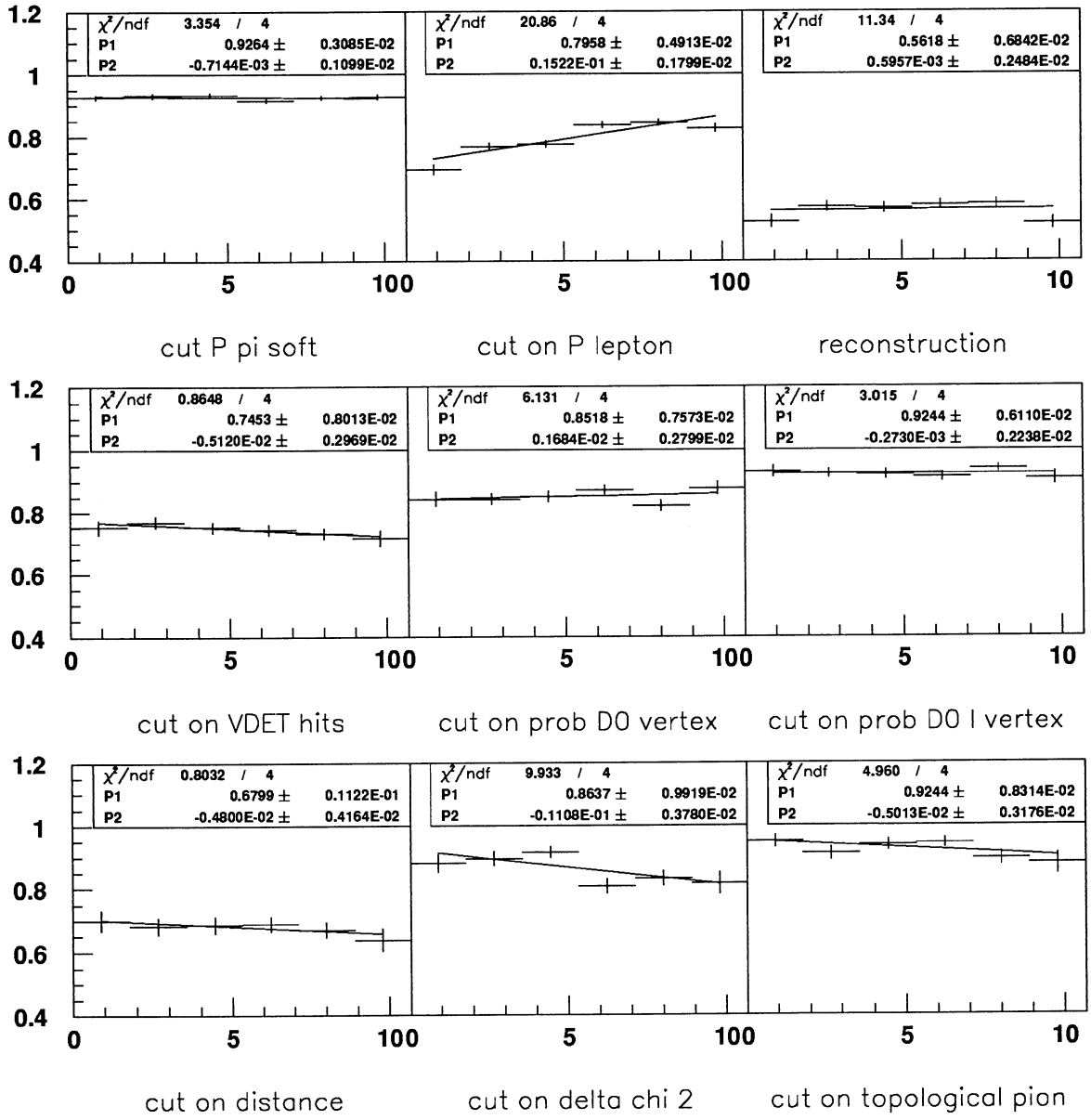

Figure 18: q^2 dependence of the efficiency of the main cuts for the $D^0 \to K^-\pi^+$ channel. The cuts of the two first plots are applied at the truth level. The third plot is the efficiency for track reconstruction and particle identification. The following ones are efficiencies of cuts applied on reconstructed quantities. Each histogram is fit with a straight line; the first parameter is the efficiency in the middle of the q^2 range and the second one is the slope.

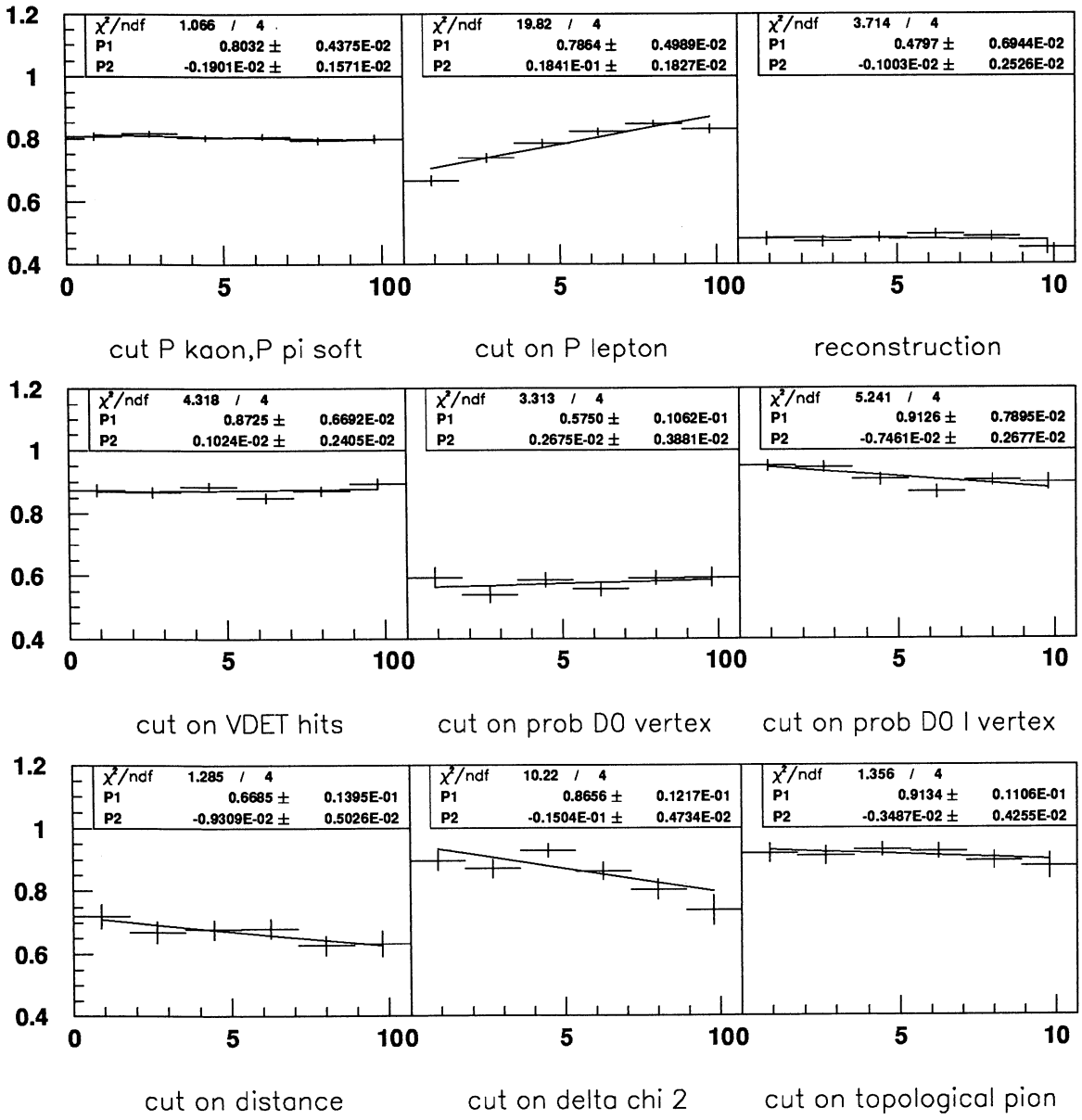

Figure 19: q^2 dependence of efficiency of the main cuts for the $D^0 \to K^-\pi^+\pi^-\pi^+$ channel. See caption of figure 18 for details.

References

[1] N. Isgur and M.B. Wise, Phys. Lett. **B 232** (1989), 113; Phys. Lett. **B 237** (1990), 527; E. Eichten and B. Hill, Phys. Lett. **B 234** (1990), 511.

[2] M.E. Luke , Phys. Lett. **B 252** (1990), 447.

[3] M. Neubert, Phys. Lett. **B 264** (1991), 455.

[4] ARGUS Collaboration H. Albrecht *et al.*, Phys. Lett. **B 275** (1992), 195; Z. Phys. **C 57**, (1993), 533; Phys. Lett. **B 324** (1994), 249; CLEO Collaboration R. Fulton *et al.*, Phys. Rev. D **43**, (1991), 651

[5] T.Browder (CLEO collaboration), to appear in Proceedings of the 27th International Conference on High Energy Physics, Glasgow, Scotland. B. Barish *et al.*, Cornell preprint CLNS **94/1285**, (1994).

[6] I. Scott, to appear in Proceedings of the 27th International Conference on High Energy Physics, Glasgow, Scotland. (see also I. Scott, A Measurement of $|V_{cb}|$from $\overline{B}^0 \rightarrow D^{*+} l^- \nu$,note for the Glasgow Conference).

[7] Particle Data Group, Phys. Rev. D 50, (1994), 1173.

[8] ALEPH Collaboration, D. Buskulic *et al.*, CERN preprint, CERN-PPE**94-173**.

[9] ALEPH Collaboration, D. Buskulic *et al.*, Phys. Lett. **B 322** (1994), 441.

[10] ALEPH Collaboration, D. Buskulic *et al.*, Phys. Lett. **B 313** (1993), 535.

[11] Review of Particle Properties, L. Montanet *et al.*, Phys. Rev. **D 50** (1994)

[12] ALEPH Collaboration, D. Buskulic *et al.*, CERN preprint, CERN-PPE**94-165**.

[13] ALEPH Collaboration, D. Buskulic *et al.*, Phys Lett. **B 322** (1994)275.

[14] Limit on B_s^0 oscillation using a jet-charge method, ALEPH Collaboration, D. Buskulic *et al.*, draft, November 1994.

[15] F.DeJongh, to appear in Proceedings of the 27th International Conference on High Energy Physics, Glasgow, Scotland

[16] M. Neubert, Phys. Lett. **B 338** (1994), 84.

[17] ALEPH Collaboration, D. Buskulic *et al.*, Z Phys. **C 62** (1994), 179.

[18] M. Neubert, Phys. Lett. **B 338** (1994), 84.

[19] S. Narison, Phys. Lett. **B 325** (1994), 197.

[20] P. Perret *et al.*, ALEPH note 94-55, Physic. 94-49.